



In silico design, synthesis and antitubercular activity of novel 2-acylhydrazono-5-arylmethylene-4-thiazolidinones as enoyl-acyl carrier protein reductase inhibitors

Serap İpek Dingiş Birgül, Jyothi Kumari, Rasoul Tamhaev, Lionel Mourey, Christian Lherbet, Dharmarajan Sriram, Atilla Akdemir, İlkay Küçükgüzel

► To cite this version:

Serap İpek Dingiş Birgül, Jyothi Kumari, Rasoul Tamhaev, Lionel Mourey, Christian Lherbet, et al.. In silico design, synthesis and antitubercular activity of novel 2-acylhydrazono-5-arylmethylene-4-thiazolidinones as enoyl-acyl carrier protein reductase inhibitors. Journal of Biomolecular Structure and Dynamics, In press, 10.1080/07391102.2024.2319678 . hal-04732279

HAL Id: hal-04732279

<https://hal.science/hal-04732279v1>

Submitted on 17 Oct 2024

HAL is a multi-disciplinary open access archive for the deposit and dissemination of scientific research documents, whether they are published or not. The documents may come from teaching and research institutions in France or abroad, or from public or private research centers.

L'archive ouverte pluridisciplinaire **HAL**, est destinée au dépôt et à la diffusion de documents scientifiques de niveau recherche, publiés ou non, émanant des établissements d'enseignement et de recherche français ou étrangers, des laboratoires publics ou privés.

IN SILICO DESIGN, SYNTHESIS AND ANTITUBERCULAR ACTIVITY OF NOVEL 2-ACYLHYDRAZONO-5-ARYLMETHYLENE-4-THIAZOLIDINONES AS ENOYL-ACYL-CARRIER-PROTEIN REDUCTASE INHIBITORS

Serap İpek Dingiş Birgül^{1,2}, Jyothi Kumari³, Rasoul Tamhaev^{4,5}, Lionel Mourey,⁵ Christian Lherbet⁴, Dharmarajan Sriram³, Atilla Akdemir⁶, İlkey Küçükgülzel^{7,*}.

¹ Marmara University, Institute of Health Sciences, Department of Pharmaceutical Chemistry, Istanbul, Turkey.

² Computer-aided Drug Discovery Laboratory, Department of Pharmacology, Bezmialem Vakif University, Istanbul, Turkey.

³ Department of Pharmacy, Birla Institute of Technology & Science Pilani, Hyderabad Campus, Hyderabad, India.

⁴ Laboratoire de Synthèse et Physico-Chimie de Molécules d'Intérêt Biologique, Université Toulouse III - Paul Sabatier, Toulouse Cedex 09, France.

⁵ Institut de Pharmacologie et de Biologie Structurale, IPBS, Université de Toulouse, CNRS, UPS, Toulouse, France;

⁶ Faculty of Pharmacy, Department of Pharmacology, Istinye University, Istanbul, Türkiye;

⁷ Department of Pharmaceutical Chemistry, Faculty of Pharmacy, Fenerbahçe University, Istanbul, Türkiye

ibirgul@bezmialem.edu.tr

jyothibits99@gmail.com

atilla.akdemir@bezmialem.edu.tr

dsriram@hyderabad.bits-pilani.ac.in

christian.lherbet@univ-tlse3.fr

rasoul.tamhaev@univ-tlse3.fr

ikucukguzel@marmara.edu.tr

Abstract

Mycobacteria regulate the synthesis of mycolic acid through the fatty acid synthase system type 1 (FAS I) and the fatty acid synthase system type-2 (FAS-II). Because mammalian cells exclusively utilize the FAS-I enzyme system for fatty acid production, targeting the FAS-II enzyme system could serve as a specific approach for developing selective antimycobacterial drugs. Enoyl-acyl carrier protein reductase enzyme (MtnhA), part of the FAS-II enzyme system, contains the NADH cofactor in its active site and reduces the intermediate. Molecular docking studies were performed on an in-house database (2200 compounds). For this study, five different crystal structures of MtnhA (PDB Code: 4TZK, 4BQP, 4DOS, 4BGE, 4BII) were used due to rotamer difference, mutation and the presence of cofactors. Molecular dynamics simulations (250 ns) were performed for the novel 2-acylhydrazono-5-arylmethylene-4-thiazolidinones derivatives selected by molecular docking studies. Twenty-three compounds selected by in silico methods were synthesized. Antitubercular activity and MtnhA enzyme inhibition studies were performed for compounds whose structures were elucidated by IR, ¹H-NMR, ¹³C-NMR, HSQC, HMBC, MS and elemental analysis.

Keywords: *Mycobacterium tuberculosis*, MtnhA inhibitor, thiazolidin-4-one, arylidene, molecular modeling, molecular dynamics.

1. INTRODUCTION

Tuberculosis is a contagious disease caused by *Mycobacterium tuberculosis* that can lead to death.¹ *M. tuberculosis* can infect other organs in the body (extrapulmonary TB) besides the lungs (pulmonary TB).² In 2021, approximately 1.6 million people, 187,000 of whom were HIV-positive, died from tuberculosis.³ *M. tuberculosis* is an aerobic bacillus classified among gram positive bacteria, although it resembles gram negative bacteria because of its second outer membrane containing mycolic acids in the cell wall.⁴

The cell wall of *M. tuberculosis* consists of two segments, the lower segment consisting of mycolyl-arabinogalactan-peptidoglycan (mAGP) core and the upper segment consisting of free lipids.⁵ All these structures in the cell wall play critical roles in cell growth, cell survival, virulence and antibiotic permeability.²

The synthesis of mycolic acid which is the essential component of mycobacterial cell wall, is controlled by two systems fatty acid synthase system type 1 (FAS I) and fatty acid synthase system type 2 (FAS II). Since eukaryotic cells produce fatty acids using only the FAS I enzyme system, the FAS II enzyme system can be an appropriate target for selective antimycobacterial drugs.⁶ The FAS II pathway, which consists of the enoyl acyl carrier protein reductase enzyme (MtnhA)⁷, is a validated target for antimycobacterial drugs.²

MtnhA is a NADH-dependent enzyme.⁸ Trans-2-enoyl-acyl carrier protein fatty acids with a chain of more than 12 carbons are reduced by MtnhA.⁹ Isoniazid (INH), which is among the first-line drugs, is an example that inhibits the mycobacterial cell wall.⁸ INH is activated by a peroxidase encoded by *katG*. The INH-NAD adduct is then formed. This adduct inhibits MtnhA. As a result, mycolic acid synthesis is blocked by the inhibition of NADH-dependent enoyl-ACP reduction, which causes cell lysis.¹⁰

It has been reported in previous publications that 4-thiazolidinone derivatives have antiviral¹¹⁻¹⁴, anticancer¹⁵, antibacterial¹⁶, and antitubercular effects¹¹. In addition, it has been reported in previous studies that compounds with arylidene structure also show anticancer¹⁵, antiviral^{13,14}, antibacterial¹¹ and antimycobacterial¹¹ activities.

It has been shown in various publications that compounds bearing the 4-thiazolidinone core have antitubercular effects (Figure 1). Küçükgül et al. reported that the compound in the *N*-[4-({2-(4-fluorophenyl)-4-oxo-1,3-thiazolidin-3-yl}amino)carbonyl]phenyl-4-methoxybenzamide structure they synthesized showed 98% inhibition against *M. tuberculosis* H37Rv at 6.25 µg/ml.¹⁷ Poyraz et al. also reported in their article that 3-((Z)-((Z)-5-(2-methoxybenzylidene)-3-methyl-4-oxothiazolidin-2-ylidene)amino)benzoic acid compound showed 96.9% inhibition against *M. tuberculosis* at 500 nM.¹⁸ Devi et al., synthesizing rhodanine derivatives, reported a compound of (Z)-*N'*-(3-(4-oxo-2-thioxo-5-(3,4,5-trimethoxybenzylidene)thiazolidin-3-yl)propanoyl)isonicotinohydrazide structure with a MIC value of 1.55 micromolar for the *M. tuberculosis* H37Rv strain.¹⁹ Slepikas et al. reported that they found the MtnhA IC₅₀ value of 2.9 for (2S)-2-((5Z)-5-[(10-chloroanthracen-9-yl)methylidene-4-oxo-2-thioxo-1,3-thiazolidin-3-yl]-3-(1*H*-indol-3-yl)propanoic acid, one of the rhodanine derivatives they synthesized.²⁰

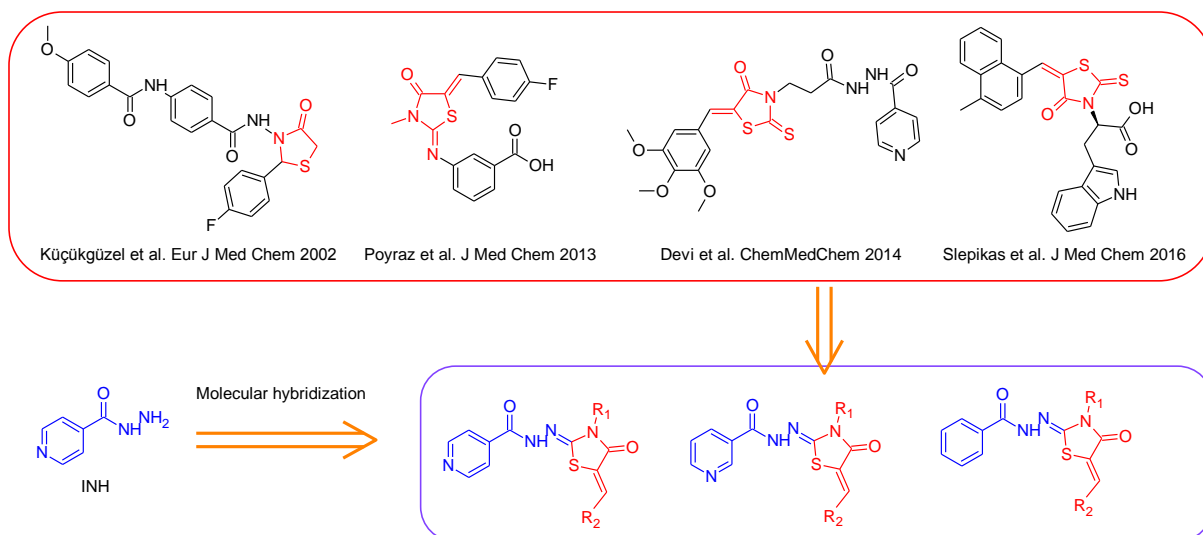


Figure 1. 4-Thiazolidinone derivatives reported for their anti-tuberculosis activity and design strategy of 2-acylhydrazono-5-arylidene-1,3-thiazolidine-4-one derivatives targeting Mtb InhA.

Here we performed molecular modelling studies on a proprietary compounds collection of 2-acylhydrazono-5-arylmethylene-4-thiazolidinones derivatives (~2200) to identify compounds that were expected to inhibit the MtbInhA enzyme. Subsequently, the selected compounds were synthesized (23 molecules) and tested in *M. tuberculosis* growth inhibition assays. Finally, a subset was tested in MtbInhA enzyme inhibition assays.

2. RESULTS AND DISCUSSION

2.1 Virtual screening studies

2.1.1 Comparison and selection of crystal structures

MtbInhA crystal structures in the PDB were investigated for use in virtual screening studies. Although it was decided to use crystal structures with and without cofactors since the binding modes of co-crystallized ligands were completely changed, it was noticed that the structures with and without cofactors also had differences within themselves (Table 1, Figure 1).

Crystal structures of MtbInhA in complex with the cofactor (NAD) as well as co-crystallized ligands (PDB entries: 4TZK; 4BQP; 4DOS) were obtained from the RCSB Protein Data Bank.²¹ Although all NAD-containing crystal structures are wild type, they have conformational differences in the side chains of Phe149 and Tyr158 residues. Therefore, there are differences in the binding modes of co-crystallized ligands.²² Side chains in the "in" position are closer to the ligand in the binding site, while the side chains in the "out" position move away from the binding site, opening a larger area for ligand placement.

Crystal structures without the cofactor but with pyridomycin (PDB entries: 4BGE; 4BII) were also obtained. The difference between the 4BII and 4BGE crystal structures is the S94A mutation located at the binding site. In the 4BGE crystal structure with the mutation, the hydrophobic alanine residue is located in the binding site instead of the polar residue serine. Thus, differences may arise in terms of bonding relationships such as hydrogen bonding or hydrophobic interaction. There are no conformational differences that affect the binding mode in these crystal structures.

Table 1. MTInhA crystal structures used in virtual screening studies and their differences.

PDB Code	Resolution (Å)	Ligand	Differences in MtlInhA crystal structures			
			NAD	Mutation	Phe149	Tyr158
4TZK	1.62	(3S)-1-cyclohexyl-N-(3,5-dichlorophenyl)-5-oxopyrrolidine-3-carboxamide	+	-	Out	In
4BQP	1.89	(1S)-1-(5-([1-(2,6-difluorobenzyl)-1H-pyrazol-3-yl]amino)-1,3,4-thiadiazol-2-yl)-1-(4-methyl-1,3-thiazol-2-yl)ethanol	+	-	Out	Out
4DOS	1.64	1-{4-[(acetylamino)methyl]phenyl}-4-(4-chlorophenoxy)-6-oxo-1,6-dihydropyridazine-3-carboxamide	+	-	In	Out
4BGE	2.25	Pyridomycin	-	S94A	Out	In
4BII	1.95	Pyridomycin	-	-	Out	In

2.1.2 Docking studies

2.1.2.1 Validation of docking protocols

Retrospective dockings were performed for all crystal structures, while enrichment graphs were created for crystal structures carrying NAD, as well as retrospective dockings (Supp. Inf. Figure 1-3).

The original binding relationships were captured by retrospective dockings in SP mode for NAD-free crystal structures (4BII, 4BGE) (See Supp. Inf. Figure 4-5). Since there are not enough molecules with cofactor-independent inhibition, score validation was not performed for crystal structures without cofactors.

In the crystal structures containing cofactors (4TZK, 4BQP, 4DOS), the binding relations observed in the crystal structures in the SP binding mode were captured. In addition, enrichment graphs were created for these crystal structures and the success of scoring in HTVS, SP and XP binding modes was tested. Since the SP binding mode is successful in both exposure capture and scoring, it was decided to be chosen as the scoring function in docking studies with all NAD-containing crystal structures.

In conclusion, pose capture in all crystal structures was confirmed by retrospective docking studies. When the poses obtained by retrospective docking of the co-crystallized ligands were compared with the co-crystallized structures, the RMSD values of the ligands were calculated as 1.5 Å below. In the light of all these studies, SP mode was used as the scoring function for all crystal structures.

2.1.2.2 Docking of in-house database

In-house database containing 2-acylhydrazono-5-arylmethylene-4-thiazolidinones derivatives (~2,200 molecules) were docked to all crystal structures in SP mode. The obtained poses were evaluated in terms of protein-ligand shape compatibility, protein-ligand binding relationships, conformation of ligands, and pose scores. As a result of the evaluation, MD simulation studies were performed for 17 poses.

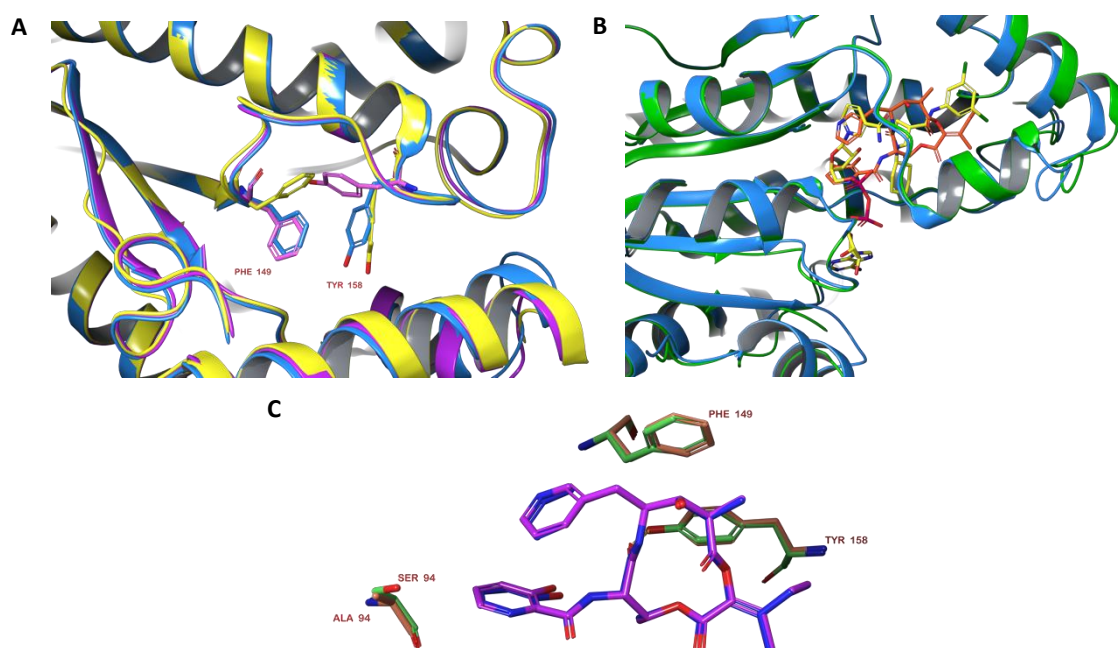


Figure 1. A) 3 crystal structures containing cofactor (4TZK in blue, 4BQP in purple, 4DOS in yellow) were superposed to see the rotamers of amino acids Tyr158 and Phe149. B) Localization of inhibitors in crystal structures with (4TZK in blue, the cofactor and inhibitor of 4TZK in yellow) and without cofactor (4BII in green, pyridomycin in orange). C) The location of the mutation in the 4BGE (shown in orange) crystal structure in the binding region is shown by overlaying 4BII (shown in green).

2.1.3 MD simulations

MD simulation studies of compound **3** and compound **17**, which show the highest activity in enzyme inhibition studies, are explained in detail below. Molecular dynamics results of compound **5** and compound **15** showing 23% and 22% enzyme inhibition respectively, are presented in the supplementary information section (See Supp. Inf. Figure 9-10). In addition to seventeen poses, MD simulations of co-crystallized structures were also performed. All simulations were run for 250 ns.

MD simulation of compound **3** with 4BGE crystal structure is shown in Figure 2. Only hydrophobic interactions were seen at the beginning of the simulation (Figure 2A). At the end of the simulation, a hydrogen bond was established between the hydrazone part of the ligand and the side chain of Tyr158. At the same time, a π - π interaction was observed between the arylidene part of the ligand and Tyr158 (Figure 2B). When the histogram of the protein-ligand interaction was examined, it is seen that the binding occurs mostly through water-mediated hydrogen bonds and hydrophobic interactions. In particular, the interaction between Ile21 and the ligand observed throughout the simulation time, and the interactions of Tyr158 with the ligand (hydrophobic, water-mediated hydrogen bonding, hydrogen bonding) observed throughout the simulation time (Figure 2C). Considering the two-dimensional protein-ligand interaction graph, it was seen that 52% of the interactions with Ile21 were water-mediated hydrogen bonds during the simulation period. Water-mediated hydrogen bonding was established with Ala22 during 37% of the simulation time. In addition, it is noteworthy that the hydrophobic interactions between Tyr158 and the ligand, which were also seen in the histogram of the interaction, are π - π interactions during 52% of the simulation time (Figure 2D). It was observed that the RMSD value of the protein was below 3 Å throughout the simulation. Although the RMSD value of the ligand (up to 4.5 Å) sometimes exceeds the RMSD value of the protein, it appears to be similar to the protein RMSD value in

most of the simulation (Figure 2E). This data suggests that the binding relationships are preserved. For this reason, it was decided to evaluate the change in the binding relationship in terms of energy by calculating the MM-GBSA binding energy throughout the simulation. When the MM-GBSA graph were inspected, it was seen that the energy ranged between 100 kcal/mol and -60 kcal/mol. It was observed that the energy level was approximately the same (-80 kcal/mol) at the beginning and at the end of the simulation (Figure 2F).

In the MD simulation performed with the co-crystallized ligand of the 4BGE crystal structure, it was seen that the hydrogen bonds established with Lys165 and Ile194 at the beginning were also at the end of the simulation. Protein α -carbons and ligand RMSD values were below 3.2 Å throughout the simulation. The average MM-GBSA binding free energy was calculated as -94.65 +/- 9.34 kcal/mol, while the maximum value was -70 kcal/mol while the minimum value was around -130 kcal/mol (See Supp. Inf. Figure 4).

MD simulation of compound **17** with 4DOS crystal structure is shown in Figure 3. At the beginning of the simulation, π - π interaction was seen between the *N*-phenethyl group of the ligand and Phe149, at the same time the ligand formed a hydrogen bond with Tyr158 via the hydrazone group (Figure 3A). Hydrophobic interactions were observed at the end of the simulation (Figure 3B). When the histogram showing the protein ligand interaction were examined, it was seen that there were interactions between Tyr158 and the ligand throughout the simulation time. Two other important interactions seen in the histogram were the hydrophobic interaction between the ligand and the amino acid Phe149 for 60% of the simulation time, and the water-mediated hydrogen bond with Glu219 for 80% of the simulation time (Figure 3C). When the two-dimensional protein ligand interaction graph was inspected, water-mediated hydrogen bonds were seen 60% of the simulation time with Tyr158 and 75% of the simulation time with Glu219. Also, the hydrophobic interactions with Phe149 seen in the histogram appear to be π - π interactions 52% of the simulation time (Figure 3D). Although the RMSD value of the protein was below 3 Å, it was seen that the RMSD value of compound **17** increases up to around 9 Å during the simulation. Therefore, it is interpreted that attachment relationships have changed (Figure 3E). In the MM-GBSA graph, it was seen that the energy varies between -40 kcal/mol and -90 kcal/mol. The energy increased towards the end of the simulation (Figure 3F).

In the MD simulation performed with the co-crystallized ligand of 4DOS crystal structure, it is seen that the hydrogen bonds established with Tyr158 at the beginning are also at the end of the simulation. The RMSD value of protein alpha-carbons was below 2.4 Å, while the RMSD value of the ligand was below 3.2 Å throughout the simulation. The average MM-GBSA binding free energy was calculated as -83.54 +/- 6.04 kcal/mol, while the maximum value was -65 kcal/mol, while the minimum value was around -106 kcal/mol (See Supp. Inf. Figure 4).

MD simulation of compound **15** with 4BII crystal structure is shown in Supp. Inf. Fig XX. In the pose at the beginning of the simulation, π - π interactions between Phe97 with the hydrazone portion of the ligand and hydrogen bonding between the endocyclic carbonyl and Ile194 are seen (See Supp. Inf. Figure 9A). Hydrophobic interactions were seen in the pose at the end of the simulation (See Supp. Inf. Figure 9B). The most important interactions in the histogram were water-mediated or direct hydrogen bonding with Phe97 that persists 60% of the simulation time, water-mediated or direct hydrogen bonding with Met98 that continues 50% of the simulation time, and water mediated or direct hydrogen bonding with Gln100 that continues 45% of the simulation time. In addition, the hydrophobic interaction with Phe149, which was observed 55% of the simulation time, is remarkable (See Supp. Inf. Figure

9C). When inspected the two-dimensional protein ligand interaction plot, it was seen that the hydrogen bond with Met98 during 47% of the simulation time and the hydrogen bond with Phe97 during 52% of the simulation time were important for binding (See Supp. Inf. Figure 9D). The RMSD value of the protein occasionally exceeds 3 Å. This suggested that there may be a conformational change in the protein. The RMSD value of compound **15** was observed to over around 4 Å throughout the simulation. In this case, it can be interpreted that the initial binding relationships of the ligand have changed (See Supp. Inf. Figure 9E). When the MM-GBSA energy graph examined, it was seen that the energy ranges between -75 kcal/mol and -110 kcal/mol throughout the simulation and increases towards the end of the simulation (See Supp. Inf. Figure 9F).

MD simulation was performed with the co-crystallized ligand of 4BII crystal structure. The hydrogen bonds between the ligand and Tyr158 and Ile194 were seen in the co-crystallized structure were not preserved throughout the simulation. The RMSD value of protein alpha-carbons was below 2.7 Å, while the RMSD value of the ligand was below 4.5 Å throughout the simulation. The average MM-GBSA binding free energy was calculated as -274.27 +/- 15.36 kcal/mol, while the maximum value was -220 kcal/mol while the minimum value was around -320 kcal/mol (See Supp. Inf. Figure 5).

MD simulation of compound **5** with 4TZK crystal structure is shown in Supp. Inf. Fig XX. When the pose at the beginning of the simulation was examined, a hydrogen bond was observed between the endocyclic carbonyl of the ligand and NAD (See Supp. Inf. Figure 10A). At the end of the simulation, this interaction was not observed, but a π - π interaction was observed between the arylidene group of the ligand and Tyr158 (See Supp. Inf. Figure 10B). When the histogram was inspected, it was seen that the binding occurs mostly with hydrophobic interactions between the ligand and protein. The most important interactions were the water-mediated hydrogen bond between the NAD-ligand, which was seen almost throughout at the simulation time, and the interactions with Tyr158, which were mostly hydrophobic for 75% of the simulation time (See Supp. Inf. Figure 10C). When the two-dimensional interaction graph was examined, it was seen that these hydrophobic interactions with Tyr158 are π - π interactions 44% of the simulation time (See Supp. Inf. Figure 10D). While the RMSD value of the protein was below 3 Å throughout the simulation, it was observed that the RMSD value of the compound **5** increased to a maximum of around 4.5 Å throughout the simulation (See Supp. Inf. Figure 10E). When the MM-GBSA graph was examined during this **increase**, it was seen that the energy also increased. In the continuation of the simulation, the RMSD value and the energy value decrease again. In the MM-GBSA graph, it was seen that while the energy reached around -85 kcal/mol at the end of the simulation, it varied between -40 kcal/mol and -90 kcal/mol throughout the simulation (See Supp. Inf. Figure 10F).

MD simulation was performed with the co-crystallized ligand of 4TZK crystal structure. The RMSD value of protein α -carbons was below 2.4 Å, while the RMSD value of the ligand was below 3.2 Å throughout the simulation. The average MM-GBSA binding free energy was calculated as -81.45 +/- 7.14 kcal/mol, while the maximum value was -59 kcal/mol while the minimum value was around -93 kcal/mol (See Supp. Inf. Figure 8).

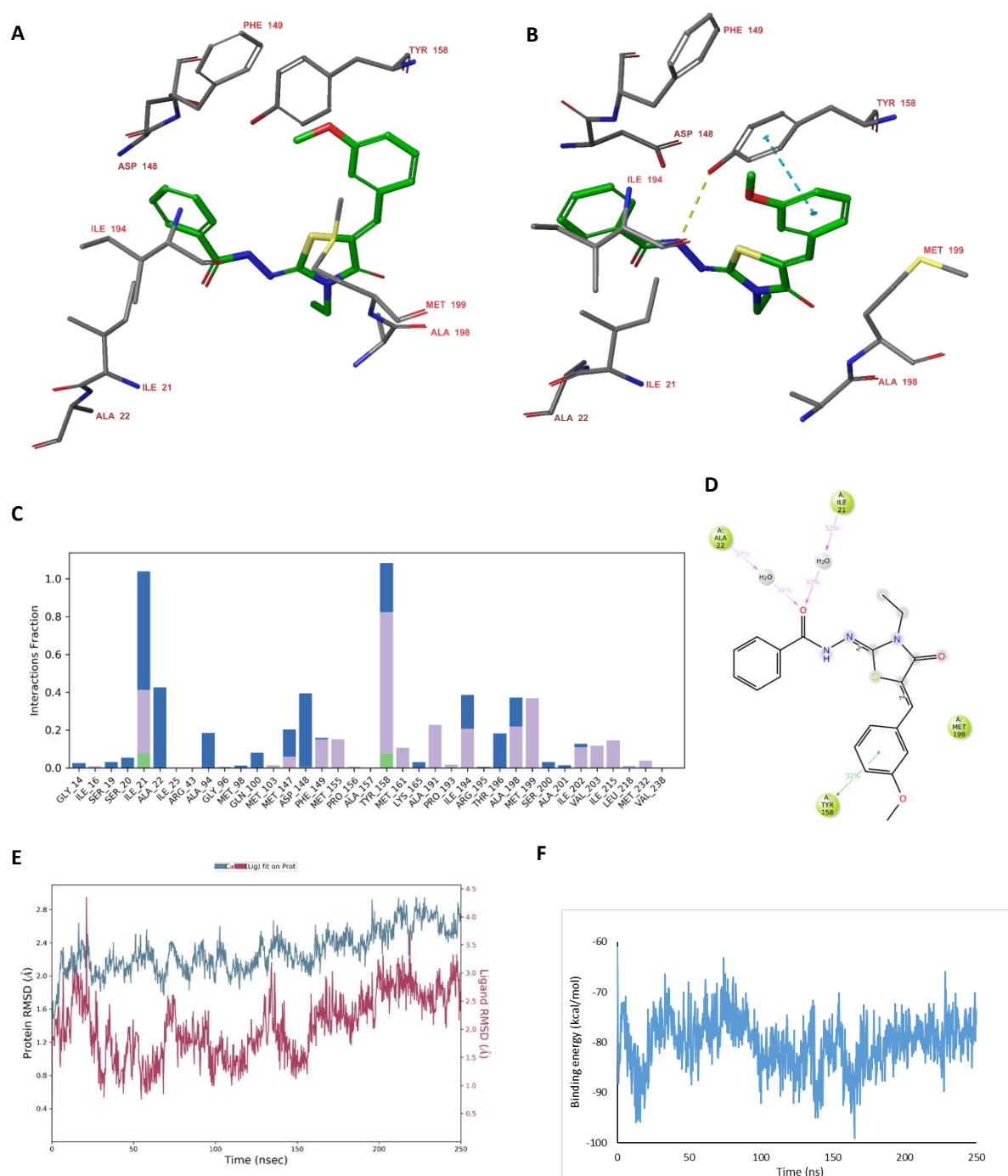


Figure 2. Molecular dynamic simulation analysis results of MtInhA (4BGE)-compound **3** complex. A) Pre-simulation (0 ns) pose of protein (4BGE) and ligand (compound **3**) complex (Green color ligand; gray color protein; dashed yellow line shows hydrogen bonding), B) At the end of simulation (250 ns) pose of protein (4BGE) and ligand (compound **3**) complex (Green color shows ligand; gray color shows protein), C) showing interaction of protein (4BGE) and ligand (compound **3**) during simulation histogram (Green color describes hydrogen bonds; purple color describes hydrophobic interactions; blue color describes water bridges), D) Two-dimensional graph showing the interaction of protein (4BGE) and ligand (compound **3**) (Green color hydrophobic amino acids; gray color water molecules; green line segment π - π interaction; purple arrows hydrogen bonds), E) RMSD values of protein (4BGE) and ligand (compound **3**) observed during simulation (Pink color indicates ligand RMSD value; blue color indicates protein RMSD value). F) Graph showing the MM-GBSA energy (kcal/mol) change throughout the simulation.

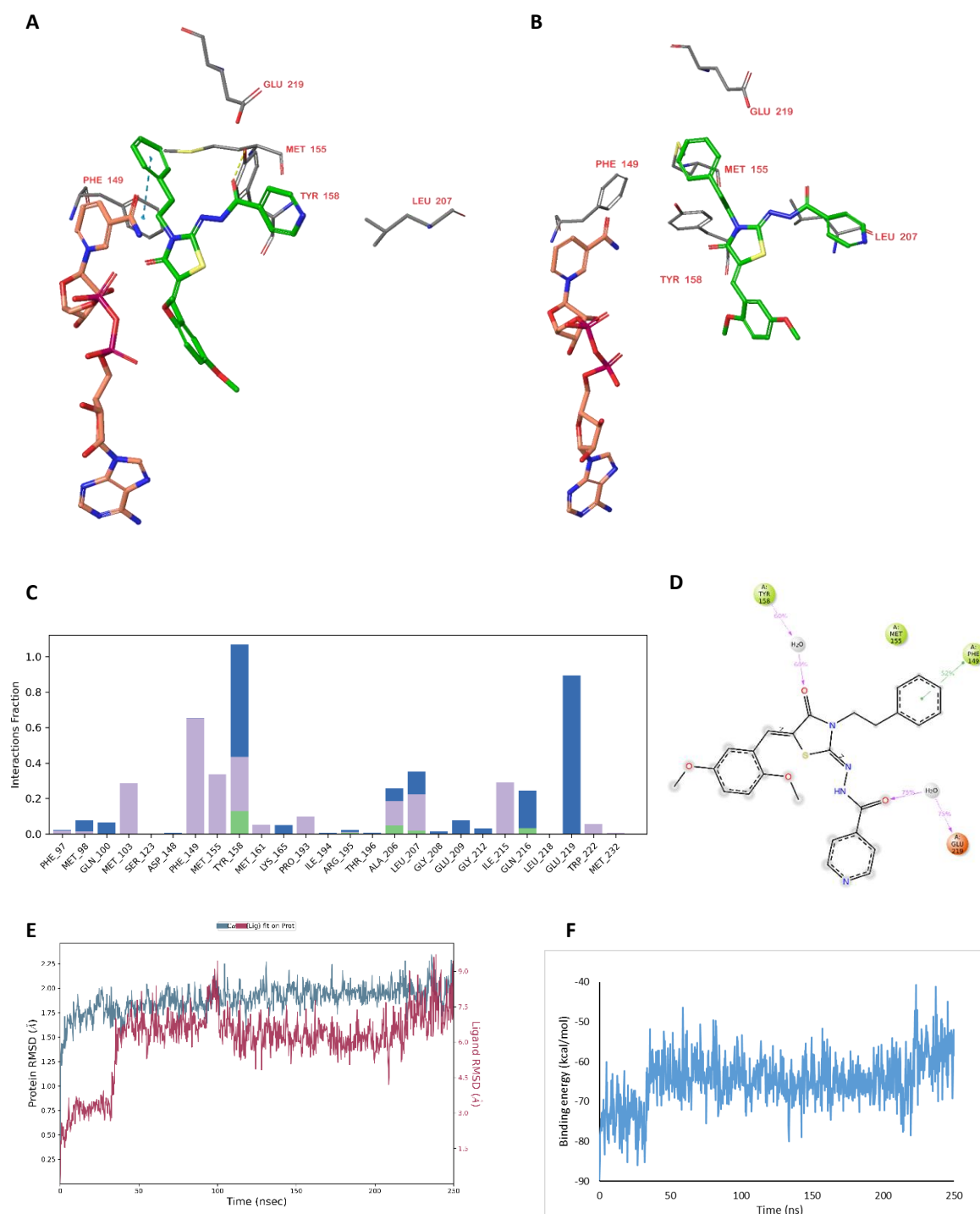


Figure 3. Molecular dynamic simulation analysis results of MtlNhA (4D0S)-compound **17** complex. A) Pre-simulation (0 ns) pose of protein (4D0S) and ligand (compound **17**) complex (Green color ligand; gray color protein; pink color cofactor (NAD); dashed yellow line shows hydrogen bonding), B) At the end of simulation (250 ns) pose of protein (4D0S) and ligand (compound **17**) complex (Green color shows ligand; gray color shows protein; pink color shows cofactor (NAD)), C) showing interaction of protein (4D0S) and ligand (compound **17**) during simulation histogram (Green color describes hydrogen bonds; purple color describes hydrophobic interactions; blue color describes water bridges), D) Two-dimensional graph showing the interaction of protein (4D0S) and ligand (compound **17**) (Green color hydrophobic amino acids; gray color water molecules; green line segment π - π interaction; purple arrows hydrogen bonds; red color negatively charged amino acids), E) RMSD values of protein (4D0S) and ligand (compound **17**) observed during simulation (Pink color indicates ligand RMSD value; blue color indicates protein RMSD value). F) Graph showing the MM-GBSA energy (kcal/mol) change throughout the simulation.

2.1.4 Selection of molecules for synthesis

As a result of virtual screening studies and MD simulations, it was decided to select 2-acylhydrazono-5-arylmethylene-4-thiazolidinone derivatives for synthesis. Different derivatives similar to the decided ligands were also synthesized.

2.1.5 *In silico* ADME predictions

ADME properties of synthesized compounds were calculated with QikProp. QikProp also offers ranges of calculated properties that are similar to 95% of known drugs. According to these ranges, the number of reactive functional groups (rtvFG) should be between 0-2. The presence of reactive functional groups may cause reactivity and toxicity problems in *in vivo* studies. The number of reactive functional groups of all compounds synthesized within the scope of this study was calculated as zero (0).

Values in the estimation of central system activities (CNS) are in the range of -2 and 2. A value of -2 indicates that it is not active in the central nervous system, while a value of 2 indicates that it is active. All compounds synthesized within the scope of this study have -2 or -1 values, so it is estimated that they will not affect the central nervous system.

The estimated IC₅₀ value for the blockade of HERG K⁺ channels (QPlogHERG), which is desired to be below -5, was calculated and it was seen that all compounds were below this value.

The QPPCaco value gives information about the intestinal-blood barrier permeability. However, in this calculation, probabilities other than active transport are not calculated. A value greater than 500 nm/sec indicates that the permeability is very good. Sixteen of the synthesized compounds have a value of over 500 nm/sec. The remaining seven compounds have a value above 400 nm/sec. In this case, it can be interpreted that the compounds will cross the gut-blood barrier to a large extent.

Estimated percent human oral absorption has been calculated for all compounds. All compounds except compound **22** were estimated to be absorbed above 91%. Compound **22**, which is predicted to have the lowest absorption, was calculated as 77.9% of the estimated human oral absorption.

According to Lipinski's rule of 5, a drug expected to be orally active should have a maximum of 5 hydrogen bond donors, a maximum of 10 hydrogen bonds, a molecular weight of less than 500 daltons, and an octanol/water partition coefficient (cLogP) of less than 5. Only one of these rules can be violated.²³ Only compound **22** violates the Lipinski's rule of 5.

2.2 Chemistry

2.2.1 Synthesis

Compounds **1-23** were synthesized in accordance with the reaction scheme given in Figure 4. Benzohydrazide (**I**), nicotinohydrazide (**II**) and 1-benzoyl/isonicotinoyl/nicotinoyl-4-alkyl thiosemicarbazides (**III-XIII**) for the synthesis of 2-acylhydrazono-5-arylmethylene-4-thiazolidinone derivatives (**1-23**) were obtained as reported in previous publications.^{11, 12} For 4-thiazolidinone ring closure, 1-benzoyl/isonicotinoyl/nicotinoyl-4-alkyl thiosemicarbazides (**III-XIII**) dissolved in ethanol were refluxed by adding ethyl bromoacetate/chloroacetic acid and, triethylamine (TEA).²⁴ The reason why TEA is preferred instead of sodium acetate is that TEA can be easily removed from the environment by using a rotary evaporator without the need for an extraction step. Thus, the reaction efficiency was also increased. In the last step, the reaction was continued without purification of the 2-acylhydrazino-4-thiazolidinones.

For this, firstly, TEA and ethanol were evaporated. Then, aromatic aldehydes, sodium methoxide and methanol were added to the medium and refluxed.^{13, 15, 25} For this reason, it is aimed to continue the reaction with a one-pot-like approach and to reach the final product by using less solvent. In addition, the synthesis method of Vicini et al. using commercially available aldehydes, sodium acetate and acetic acid was not applied in the last step of this study. Instead of this method, sodium methoxide in methanolic medium was used with aromatic aldehydes in accordance with Knoevenagel's reaction procedure, thus shortening the reaction time. The resulting solid was crystallized from ethanol.²⁶ As a result, pure derivatives of 2-acylhydrazono-5-arylmethylene-4-thiazolidinone (**1-23**) were obtained.

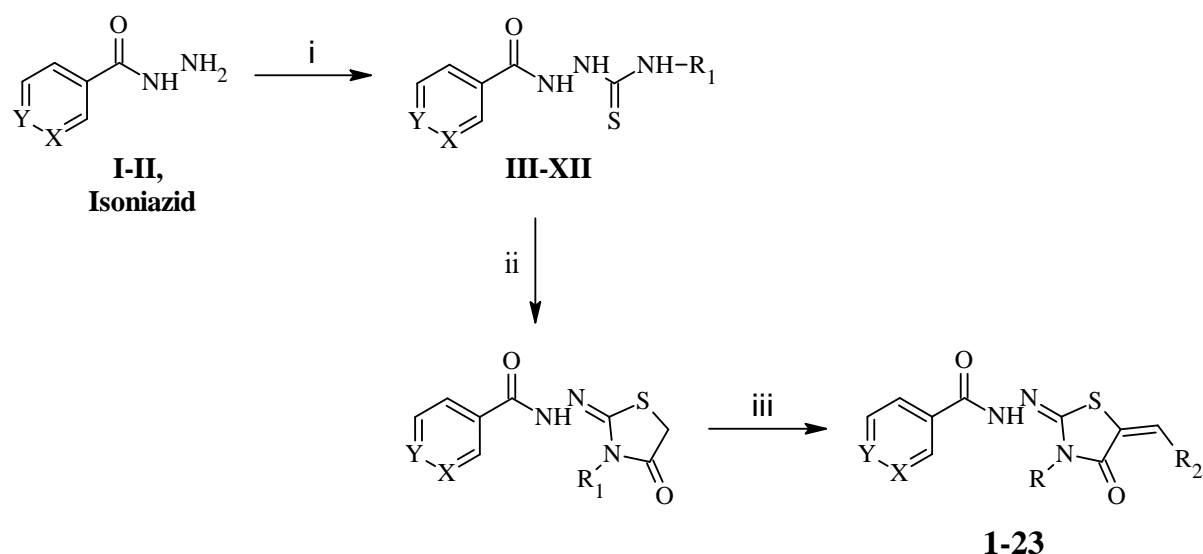


Figure 4. Synthetic route to 2-acylhydrazono-5-arylmethylene-4-thiazolidinones **1-23**. Key to the reagents and conditions: i) R₁-N=C=S, EtOH, reflux; ii) Br-CH₂-CO₂Et, TEA, EtOH, reflux; iii) R₂-CH=O, NaOMe, MeOH, reflux.

2.2.2 Structure characterization

Purities of all compounds were checked by TLC. Reaction monitoring was also performed with TLC. In addition, the purity of the compounds **1-23** was checked by elemental analysis. Melting degrees of all compounds were determined. FT-IR, ¹H-NMR, ¹³C-NMR, MS spectra were obtained for compounds **1-23**. In addition, HSQC and HMBC spectra for compound **16** were obtained and the structure was elucidated in detail.

In the FT-IR spectra, -NH- stretching bands of compounds **1-23** were seen in the range of 3062 to 3221 cm⁻¹. Carbonyl (C=O) stretching bands were also observed around 1600-1700 cm⁻¹ for compounds **1-23**.¹⁵

When the ¹H-NMR spectra of compounds **1-23** were examined, it was observed that the shift values of all recorded protons were as expected. In ¹H-NMR, the chemical shift value of -NH-, which is common to all structures, is around 11 ppm. Only in the compound **13** and compound **14** spectra, proton and deuterium were exchanged and the -NH- peak could not be seen. "=CH-Ar" peaks were observed between 7-8 ppm in the aromatic field.¹³ The fact that S-CH₂- protons, which are expected to be seen in 2-acylhydrazino-4-thiazolidinone derivatives, are not seen in the compound **1-23** spectra supports that 2-acylhydrazino-4-thiazolidinone compounds are not left in the medium at the end of the synthesis.²⁵ While the methine proton has high shift values in Z isomers, it has lower shift values in E isomers due to the deshielding effect of sulfur. Therefore, it was supported by ¹H-NMR that compounds **1-23** were found as the Z isomer.¹³

When the ^{13}C -NMR spectra of compounds **1-23** were examined, it was observed that the chemical shift values of all recorded protons were as expected. In the ^{13}C -NMR spectra, the exocyclic carbonyl resonances were seen around 162-164 ppm, in the lower energy area than the endocyclic carbonyl carbons. The carbons of endocyclic carbonyls were found to be around 164-166 ppm²⁷. Thiazolidinone C2 carbons resonated in the range of 150-158 ppm, while thiazolidinone C5 carbons appeared in the range of 121-126 ppm. Finally, the =CH-Ar peaks common to all structures were recorded in the range of 125-129 ppm in ^{13}C -NMR.¹³

HMBC and HSQC spectra for compound **16** were obtained. In the HSQC spectrum, the C-H contours of the methoxy groups are seen at 3.73 ppm - 56.03 ppm (-O-CH₃(5)) and 3.83 ppm - 56.60 ppm (-O-CH₃(2)). The contours of the =CH- group are seen at 7.93 ppm - 126.10 ppm. In the HMBC spectrum, -CH₂- hydrogens with benzyl C2-C6, benzyl C1, thiazolidinone C2 and endocyclic C=O carbons gave 5.10 ppm - 128.38 ppm, 5.10 ppm - 136.20 ppm, 5.10 ppm - 156.29 ppm and 5.10 ppm - 165.79 ppm respectively. The hydrogen of the =CH- group observed at 7.91 ppm and the carbon of the endocyclic C=O group observed at 165.81 ppm formed the contour.

Positive and negative ion APCI mass spectra of all compounds were recorded. Comparing the calculated and experimental m/z values of compounds **1-23** it was determined that there was less than 5 mu difference.

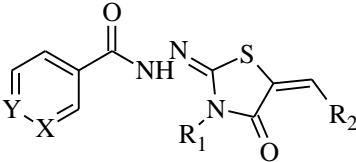
2.3 In vitro studies

According to the antimycobacterial activity results, **12** and **22** were identified as the most active compounds with a MIC value of 6.25 µg/mL. This is followed by compound **16** with 12.5 µg/mL. When these data are compared with MtlInhA inhibitions, there is no correlation between the results. Compound **12** and compound **22** showed only 21% and 22% inhibition at 50 µM, respectively. Compound **3** is the most active compound in MtlInhA inhibitions, but the minimum inhibitory concentration is higher than 25 µg/mL.

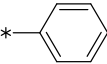
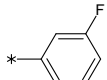
According to the MIC values of the compounds, it was observed that the derivatives containing benzyl or phenethyl at the R₁ position were more active. Additionally, in the R₂ position, ortho-substituted arylidene compounds activity is higher than other compounds (Table 2).

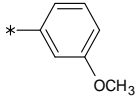
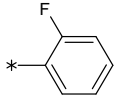
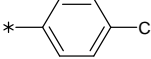
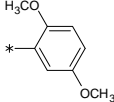
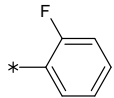
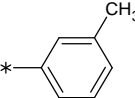
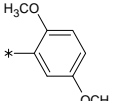
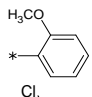
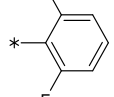
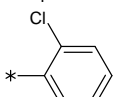
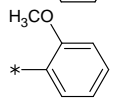
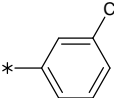
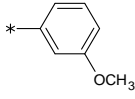
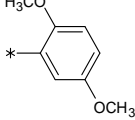
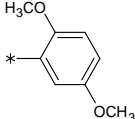
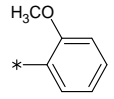
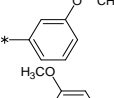
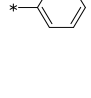
These results may be due to solubility problems and/or low permeability. In addition, compounds with a low percentage of enzyme inhibition, but with a low MIC value, may have shown activity against other targets together with the MtlInhA enzyme.

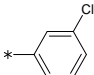
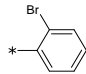
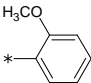
Table 2. Antimycobacterial activity and enzyme inhibition values of the compounds.



1-23

Compound	X	Y	R ₁	R ₂	MIC (µg/mL)	MIC (µM)	InhA Inhibition % at 50 µM
1	CH	CH	Ethyl		>25	NA	NA
2	CH	CH	Ethyl		25	67.67	NA (Solubility problem)

3	CH	CH	Ethyl		>25	NA	51
4	CH	CH	Allyl		>25	NA	NA
5	CH	CH	Allyl		>25	NA	23
6	CH	CH	Allyl		>25	NA	NA
7	CH	CH	Benzyl		>25	NA	5
8	CH	CH	Phenethyl		>25	NA	NA
9	CH	N	Propyl		>25	NA	17
10	CH	N	Allyl		25	63.22	4
11	CH	N	Allyl		>25	NA	NA
12	CH	N	Benzyl		6.25	13.92	21
13	CH	N	Benzyl		>25	NA	NA
14	CH	N	Benzyl		25	55.69	12
15	CH	N	Benzyl		>25	NA	22
16	CH	N	Benzyl		12.5	26.34	NA (Solubility problem)
17	CH	N	Phenethyl		>25	NA	39
18	N	CH	Propyl		>25	NA	NA
19	N	CH	Propyl		>25	NA	19
20	N	CH	Benzyl		25	56.24	13

21	N	CH	Benzyl		>25	NA	NA
22	N	CH	Phenethyl		6.25	12.32	22
23	N	CH	Phenethyl		>25		NA
Isoniazid					0.05 (µg/mL)		
Rifampicin					0.1 (µg/mL)		
Ethambutol					1.56 (µg/mL)		

NA: Not applicable.

3. EXPERIMENTAL STUDIES

3.1 Virtual screening studies

All modelling studies were performed using the Schrödinger package (v2021-1, Schrödinger, Inc., New York).

3.1.1 Ligand preparation

A proprietary compound library (~2,200 molecules) was created with the “3D Builder” module of the Schrödinger package. Subsequently, all stereoisomers and protomers (possible states at pH=7.0 +/- 2.0) were obtained using the LigPrep tool and the compounds were energy minimized using the OPLS4 force field.

3.1.2 Protein preparation

Selected crystal structures of InhA enzyme (PDB entries: 4TZK, 4DOS, 4BQP, 4BGE, 4BII) were obtained from the RCSB Protein Data Bank²¹ and prepared for molecular modelling procedures. To this end, all water molecules and ions were removed. The first protein chains were retained when more than one MtlInhA chain was available, except for the 4BII structure. The D chain was retained for 4BII, as it is the only chain that does not contain cofactors. If present, NAD was retained hydrogen atoms were added using the Protein Preparation Workflow.

3.1.3 Docking studies

3.1.3.1 Validation

26 inhibitors with different skeletons, which are located at the binding site in MtlInhA crystal structures in the protein database and have been reported to show high inhibition, were selected for validation of NAD-containing crystal structures. 520 decoy molecules similar to these molecules in terms of number of hydrogen bond donors, number of hydrogen bond acceptors, TPSA, molecular weight, molecular charge and single rotatable bonds were selected from the "Schrödinger drug like decoys 400 mw" file (See Supp Inf. XX).

All these molecules were docked into 4TZK, 4BQP and 4DOS crystal structures in HTVS, SP and XP mode, respectively. First of all, a grid was created by choosing the cocrystallized ligand. Rotatable bonds of the protein closer than 5 Å to the ligand in the grid were determined. Molecules were docked 25 times for HTVS and SP binding modes and 10 times for XP binding mode. Only the best poses of all molecules were recorded. Scores obtained for each calculation method were ordered from high to low and enrichment graphs were created.

Because the number of known inhibitors that can be used for the validation of NAD-free crystal structures is too few, enrichment graphs could not be created. Instead, they were validated with retrospective docking studies.

3.2.3.2 Docking Studies

The prepared ligands were docked into the binding sites of 4TZK, 4BQP, 4DOS, 4BGE and 4BII crystal structures using validated methods. The three best scoring poses were kept for visual inspection.

3.1.4 Molecular dynamics simulations

Desmond software (v2021-1, Schrödinger, Inc., New York) was used for molecular dynamics simulation studies. The protein-ligand complex is placed inside the orthorhombic box in periodic boundary conditions. The system was solved by adding TIP5P water molecules and neutralized by adding counter ions. The system was minimized by using the OPLS4 force field for 100 ps, keeping the protein, ligand and cofactor constant. Then, the whole system was released and molecular dynamics simulations were performed at constant temperature (300 K, Nose-Hoover Chain, default values) and pressure (1 bar, Martyna-Tobias-Klein, default values) for 250 ns.

3.1.6 In silico ADME predictions

The ADME properties given in the supplementary data were calculated using the QikProp tool included in the Schrödinger software package (v2021-1, Schrödinger, Inc., New York).

3.2 Chemistry

3.2.1 Chemical material and apparatus

Isoniazid (Sigma Aldrich), ethyl nicotinate (Sigma Aldrich), benzoic acid (Merck), substituted isothiocyanate derivatives (Sigma Aldrich), ethyl bromoacetate (Sigma Aldrich), TEA (Sigma Aldrich), hydrazine hydrate (Sigma Aldrich), methanol (Sigma Aldrich), substituted aromatic aldehyde derivatives (Sigma Aldrich), ethanol (Sigma Aldrich), glacial acetic acid (g. AcOH) (Riedel de Haen), petroleum ether (Merck), sodium methoxide.

RADLEYS parallel synthesis system was used for synthesis. Heidolph Hei-VAP Precision rotary evaporator was used to remove the solvents. Reaction monitoring and purity controls of the compounds were performed using Merck silica gel 60 F₂₅₄ plates by TLC method. Elemental analyzes of the compounds were performed using the LECO CHNS-932 instrument. The melting points of the compounds were determined with the Schmelzpunkt Bestimmer SMP II device and uncorrected. Infrared spectra of the compounds were obtained with the Shimadzu IR Affinity 1S-FTIR Instrument. NMR spectra of compounds were obtained with Bruker 400MHz AV model NMR spectrometer. The mass spectra were recorded on Shimadzu LC-MS/MS-8030 system (Shimadzu Corporation, Kyoto, Japan).

3.2.2 Synthesis

3.2.2.1 General procedure for the synthesis of hydrazides (I-II)

Benzohydrazide and nicotinohydrazide were synthesized as reported in the previous literature.¹² Isoniazid was purchased from Sigma Aldrich.

3.2.2.2 General procedure for the synthesis of thiosemicarbazides (III-XIII)

1 mmol of benzohydrazide/isoniazid/nicotinohydrazide was dissolved in ethanol. 1 mmol of the corresponding substituted isothiocyanate was added to the medium. The reaction medium was heated and stirred under reflux. At the end of the reaction, the reaction medium was cooled. The precipitated solid was collected by filtration. It is crystallized from ethanol.

3.2.2.3 Synthesis of 2-acylhydrazono-5-arylmethylene-4-thiazolidinone derivatives (**1-23**)

1 mmol of *N*-substituted thiosemicarbazide compound was dissolved in ethanol. 1 mmol of TEA and 1 mmol of ethylbromoacetate or 1 mmol of chloroacetic acid was added to the medium. The reaction medium was heated and stirred under reflux. At the end of the reaction, excess solvent and TEA were evaporated under reduced pressure. Synthesis was continued in the same pot without isolation of the corresponding 4-thiazolidinones. The flask content was heated for half an hour under reflux in methanol (made up to 12 ml) in the presence of sodium methoxide (1.46 ml) for 1-6 hours. Then aromatic aldehyde was added to the medium and heating was continued for 8 hours. At the end of the reaction, excess solvent was evaporated. Then it was neutralized with 5% acetic acid and washed with plenty of water. It was left to dry. The dried substance was then recrystallized from ethanol.

3.2.3 Structure characterization

3.2.3.1 Hydrazide derivatives (**I-II**)

Benzohydrazide (I)

CAS Number: 613-94-5, M.p. 115-116 °C (lit. 116-118 °C).²⁸

Nicotinohydrazide (II)

CAS Number: 553-53-7, M.p. 160-162 °C (lit. 164-167 °C).²⁸

3.2.3.2 Thiosemicarbazide derivatives (**III-XIII**)

1-Benzoyl-4-ethyl thiosemicarbazide (III)

CAS Number: 26257-93-2, M.p. 192-194 °C (lit. 189-192 °C).²⁹

1-Benzoyl-4-allyl thiosemicarbazide (IV)

CAS Number: 26029-04-9, M.p. 180-182 °C (lit. 185 °C).³⁰

1-Benzoyl-4-benzyl thiosemicarbazide (V)

CAS Number: 120811-69-0, M.p. 200-201 °C (lit. 193-195 °C).³¹

1-Benzoyl-4-phenethyl thiosemicarbazide (VI)

CAS Number: 77516-55-3, M.p. 190-191 °C.

1-Isonicotinoyl-4-propyl thiosemicarbazide (VII)

CAS Number: 94646-91-0, M.p. 206-208 °C (lit. 206-207 °C).³²

1-Isonicotinoyl-4-allyl thiosemicarbazide (VIII)

CAS Number: 15886-23-4, M.p. 225-227 °C (lit. 227-230 °C).³³

1-Isonicotinoyl-4-benzyl thiosemicarbazide (IX)

CAS Number: 63932-07-0, M.p. 241-242 (lit. 232 °C).³⁴

1-Isonicotinoyl-4-phenethyl thiosemicarbazide (X)

CAS Number: 13921-63-6, M.p. 242-244 °C (lit. 212 °C).³⁵

1-Nicotinoyl-4-propyl thiosemicarbazide (XI)

CAS Number: 890887-46-4, M.p. 228-230 °C.

1-Nicotinoyl-4-benzyl thiosemicarbazide (XII)

CAS Number: 211572-59-7, M.p. 190-191 °C (lit. 195-196 °C).³⁶

1-Nicotinoyl-4-phenethyl thiosemicarbazide (XIII)

CAS Number: 188182-35-6, M.p. 178-180 °C (lit. 171 °C).³⁷

3.2.3.3 2-Acylhydrazono-5-arylmethylene-4-thiazolidinones derivatives (1-23)

N'-[5-Benzylidene-3-ethyl-4-oxo-1,3-thiazolidin-2-ylidene]benzohydrazide (1)

Light yellow powder. M.p. 195-197 °C. Elemental analysis calculated for C₁₉H₁₇N₃O₂S.2/3H₂O: C 62.79, H 5.08, N 11.56, S 8.82; found: C 62.42, H 4.703, N 11.89, S 8.665. IR (cm⁻¹): 3140 (N-H); 1705, 1639 (C=O). ¹H NMR δ ppm (400 MHz, DMSO- d₆, TMS): 1.28 (t, 3H, J₁= 6.8 Hz, J₂= 7.2 Hz, CH₂-CH₃); 3.95 (q, 2H, J₁=6.8 Hz, J₂=7.2 Hz, CH₂-CH₃); 7.44-8.03 (m, 11H, =CH-Ar, Ar-H); 11.23 (s, 1H, NH-N). ¹³C NMR (100 MHz) (DMSO-d₆/TMS) δ ppm: 12.86 (-CH₂-CH₃); 38.60 (>N-CH₂-); 121.40 (thiazolidinone C5); 127.99 (=CH-, arylidene C4); 128.98 (benzohydrazide C2, C6); 129.81 (arylidene C3, C5); 130.41 (benzohydrazide C3, C5); 130.56 (arylidene C2, C6); 132.17 (benzohydrazide C4); 133.42 (arylidene C1); 133.74 (benzohydrazide C1); 156.77 (thiazolidinone C2); 164.05 (exocyclic C=O); 165.70 (endocyclic C=O). MS (APCI⁺) m/z calculated for C₁₉H₁₇N₃O₂S [M+H]⁺, 352.11; found 352.20.

N'-[5-(3-Fluorobenzylidene)-3-ethyl-4-oxo-1,3-thiazolidin-2-ylidene]benzohydrazide (2)

Light yellow powder. M.p. 179-180 °C. Elemental analysis calculated for C₁₉H₁₆FN₃O₂S: C 61.77, H 4.37, N 11.37, S 8.68; found: C 61.51, H 4.108, N 11.31 S 8.263. IR (cm⁻¹): 3147 (N-H); 1705, 1647 (C=O). ¹H NMR δ ppm (400 MHz, DMSO- d₆, TMS): 1.28 (t, 3H, J₁= 7.2 Hz, J₂= 7.2 Hz, CH₂-CH₃); 3.95 (q, 2H, J₁=6.8 Hz, J₂=7.2 Hz, CH₂-CH₃); 7.32-7.91 (m, 10H, =CH-Ar, Ar-H); 11.24 (s, 1H, NH-N). ¹³C NMR (100 MHz) (DMSO-d₆/TMS) δ ppm: 12.83 (-CH₃); 38.69 (>N-CH₂-); 117.11-117.23 (arylidene C4); 117.23-117.34 (arylidene C2); 123.08 (thiazolidinon C5); 125.84 (arylidene C6); 128.04 (=CH-); 128.99 (benzohydrazide C2, C6); 129.24 (benzohydrazide C3, C5); 131.90 (arylidene C5); 132.22 (benzohydrazide C4); 133.47 (arylidene C1); 136.16 (benzohydrazide C1); 156.07 (thiazolidinone C2); 161.52-163.96 (arylidene C3); 164.24 (exocyclic C=O); 165.46 (endocyclic C=O). MS (APCI⁻) m/z calculated for C₁₉H₁₆FN₃O₂S [M-H]⁻, 368.09; found 368.15.

N'-[5-(3-Methoxybenzylidene)-3-ethyl-4-oxo-1,3-thiazolidin-2-ylidene]benzohydrazide (3)

Light yellow powder. M.p. 175-178 °C. Elemental analysis calculated for C₂₀H₁₉N₃O₃S.1/3H₂O: C 62.00, H 5.12, N 10.85, S 8.28; found: C 62.25, H 4.823, N 11.03, S 8.084. IR (cm⁻¹): 3147 (N-H g.b.); 1712, 1643 (C=O g.b.). ¹H NMR δ ppm (400 MHz, DMSO- d₆, TMS): 1.28 (t, 3H, J₁= 6.8 Hz, J₂= 6.8 Hz, CH₂-CH₃); 3.88 (q, 5H, CH₂-CH₃, Ar-OCH₃); 7.05-7.91 (m, 11H, =CH-Ar, Ar-H); 11.22 (s, 1H, NH-N). ¹³C NMR (100 MHz) (DMSO-d₆/TMS) δ ppm: 12.84 (-CH₃); 38.58 (>N-CH₂-); 55.72 (-O-CH₃); 116.08 (arylidene C4); 116.36 (arylidene C2); 121.74 (arylidene C6);

121.93 (thiazolidinone C5); 128.02 (=CH-); 128.98 (benzohydrazide C2, C6); 130.59 (benzohydrazide C3, C5); 130.92 (arylidene C5); 132.19 (benzohydrazide C4); 133.53 (arylidene C1); 135.09 (benzohydrazide C1); 156.41 (thiazolidinone C2); 160.06 (arylidene C3); 164.01 (exocyclic C=O); 165.56 (endocyclic C=O). MS (APCI⁻) m/z calculated for C₂₀H₁₉N₃O₃S [M-H]⁻, 380.11; found 380.20.

N'-[5-(2-Fluorobenzylidene)-3-allyl-4-oxo-1,3-thiazolidin-2-ylidene]benzohydrazide (4)

Light yellow powder. M.p. 174-176 °C. Elemental analysis calculated for C₂₀H₁₆FN₃O₂S.1/3H₂O: C 62.00, H 4.34, N 10.85, S 8.28; found: C 62.16, H 4.344, N 10.99, S 8.054. IR (cm⁻¹): 3197 (N-H); 1705, 1651 (C=O). ¹H NMR δ ppm (400 MHz, DMSO- d₆, TMS): 4.54 (s, 2H, N-CH₂-CH-); 5.24 (d, 2H, J=8.8 Hz, -CH=CH₂); 5.97 (m, 1H, CH₂-CH=CH₂); 7.39 – 7.91 (m, 10H, Ar-H, =CH-Ar); 11.27 (s, 1H, NH-N). ¹³C NMR (100 MHz) (DMSO-d₆/TMS) δ ppm: 45.44 (>N-CH₂-); 116.57-116.78 (arylidene C3); 118.07 (=CH₂); 121.52-121.64 (arylidene C1); 123.93 (thiazolidinone C5); 125.92 (arylidene C4); 125.95 (arylidene C5); 128.02 (=CH-); 128.98 (benzohydrazide C2, C6); 129.45 (benzohydrazide C3, C5); 131.38 (arylidene C6); 132.85 (benzohydrazide C4); 132.94 (-CH=CH₂); 133.39 (benzohydrazide C1); 156.07 (thiazolidinone C2); 159.58-162.08 (arylidene C2); 164.07 (exocyclic C=O); 165.29 (endocyclic C=O). MS (APCI⁺) m/z calculated for C₂₀H₁₆FN₃O₂S [M-H]⁺, 380.09; found 380.20.

N'-[5-(4-Chlorobenzylidene)-3-allyl-4-oxo-1,3-thiazolidin-2-ylidene]benzohydrazide (5)

Light yellow powder. M.p. 237-240 °C. Elemental analysis calculated for C₂₀H₁₆ClN₃O₂S.1/2H₂O: C 59.04, H 4.21, N 10.33, S 7.88; found: C 59.26, H 4.071, N 10.08, S 7.726. IR (cm⁻¹): 3132 (N-H); 1705, 1651 (C=O). ¹H NMR δ ppm (400 MHz, DMSO- d₆, TMS): 4.53 (d, 2H, J=5.2 Hz, N-CH₂-CH-); 5.24 (d, 2H, J=12.8 Hz, -CH=CH₂); 5.96 (m, 1H, CH₂-CH=CH₂); 7.26 – 7.92 (m, 10H, Ar-H, =CH-Ar); 11.26 (s, 1H, NH-N). ¹³C NMR (100 MHz) (DMSO-d₆/TMS) δ ppm: 45.36 (>N-CH₂-); 117.95 (=CH₂); 121.98 (thiazolidinone C5); 128.00 (=CH-); 128.97 (benzohydrazide C2, C6); 129.48 (benzohydrazide C3, C5); 129.89 (arylidene C3, C5); 129.94 (arylidene C1); 131.45 (arylidene C2, C6); 132.10 (benzohydrazide C4); 132.63 (-CH=CH₂); 133.38 (benzohydrazide C1); 135.11 (arylidene C4); 156.12 (thiazolidinone C2); 163.86 (exocyclic C=O); 165.50 (endocyclic C=O). MS (APCI⁺) m/z calculated for C₂₀H₁₆ClN₃O₂S [M+H]⁺, 398.07; found 398.15.

N'-[5-(2,5-Dimethoxybenzylidene)-3-allyl-4-oxo-1,3-thiazolidin-2-ylidene]benzohydrazide (6)

Yellow powder. M.p. 176 °C. Elemental analysis calculated for C₂₂H₂₁N₃O₄S: C 62.40, H 5.00, N 9.92, S 7.57; found: C 62.33, H 5.102, N 9.998, S 7.383. IR (cm⁻¹): 3221 (N-H); 1705, 1654 (C=O). ¹H NMR δ ppm (400 MHz, DMSO- d₆, TMS): 3.74 (s, 3H, Ar-(5)OCH₃); 3.96 (s, 3H, Ar-(2)OCH₃); 4.59 (d, 2H, -CH₂-CH-); 5.31 (d, 2H, J=16 Hz, -CH=CH₂); 6.02 (t, 1H, CH₂-CH=CH₂); 7.04 – 7.98 (m, 10H, Ar-H, =CH-Ar); 11.28 (s, 1H, NH-N). ¹³C NMR (100 MHz) (DMSO-d₆/TMS) δ ppm: 45.23 (-CH₂-); 56.00 (-O-CH₃(5)); 56.59 (-O-CH₃(2)); 113.40 (arylidene C4); 114.67 (arylidene C6); 116.93 (arylidene C3); 117.95 (=CH₂); 121.78 (arylidene C1); 122.81 (thiazolidinone C5); 125.44 (=CH-); 127.97 (benzohydrazide C2, C6); 128.98 (benzohydrazide C3, C5); 131.48 (benzohydrazide C4); 132.15 (-CH=CH₂); 133.55 (benzohydrazide C1); 152.60 (arylidene C2); 153.46 (arylidene C5); 156.00 (thiazolidinone C2); 164.10 (exocyclic C=O); 165.50 (endocyclic C=O). MS (APCI⁺) m/z calculated for C₂₂H₂₁N₃O₄S [M+H]⁺, 424.13; found 424.20.

N'-[5-(2-Fluorobenzylidene)-3-benzyl-4-oxo-1,3-thiazolidin-2-ylidene]benzohydrazide (7)

Light yellow powder. M.p. 191-193 °C; Elemental analysis calculated for $C_{24}H_{18}FN_3O_2S \cdot 1/4H_2O$: C 66.12, H 4.28, N 9.64, S 7.35; found: C 66.27, H 4.112, N 9.836, S 7.216. IR (cm^{-1}): 3213 (N-H); 1712, 1647 (C=O). 1H NMR δ ppm (400 MHz, DMSO- d_6 , TMS): 5.12 (s, 2H, CH_2 -Ar); 7.32 – 7.91 (m, 15H, =CH-Ar, Ar-H); 11.29 (s, 1H, NH-N). ^{13}C NMR (100 MHz) (DMSO- d_6 /TMS) δ ppm: 46.59 ($-CH_2-$); 116.58-116.79 (arylidene C3); 121.63- 122.09 (arylidene C1); 123.83 (thiazolidinone C5); 125.96 (arylidene C4); 128.03-128.22 (arylidene C5); 128.23 (=CH-); 128.34 (benzyl C4); 128.97 (benzyl C2,C6); 129.05 (benzohydrazide C2, C6); 129.48 (benzyl C3,C5); 129.49 (benzohydrazide C3, C5); 132.24 (arylidene C6); 133.01 (benzohydrazide C4); 133.30 (benzohydrazide C1); 136.14 (benzyl C1); 156.20 (thiazolidinone C2); 162.08-159.58 (arylidene C2); 164.12 (exocyclic C=O); 165.64 (endocyclic C=O). MS (APCI $^+$) m/z calculated for $C_{24}H_{18}FN_3O_2S$ $[M+H]^+$, 432.11; found 432.20.

N'-[5-(3-Methylbenzylidene)-3-phenethyl-4-oxo-1,3-thiazolidin-2-ylidene]benzohydrazide (8)

Light yellow powder. M.p. 190 °C. Elemental analysis calculated for $C_{26}H_{23}N_3O_2S$: C 70.72, H 5.25, N 9.52, S 7.26; found: C 70.66, H 5.448, N 9.662, S 7.100. IR (cm^{-1}): 3155 (N-H); 1743, 1705 (C=O). 1H NMR δ ppm (400 MHz, DMSO- d_6 , TMS): 2.43 (s, 3H, Ar- CH_3); 3.18 (t, 2H, CH_2 -Ar); 4.21 (s, 2H, N- CH_2); 7.31 – 7.04 (m, 15H, =CH-Ar, Ar-H); 11.38 (s, 1H, NH-N). ^{13}C NMR (100 MHz) (DMSO- d_6 /TMS) δ ppm: 21.41 ($-CH_3$); 32.63 ($-CH_2$ -Ar); 44.53 ($>N-CH_2-$); 123.32 (thiazolidinone C5); 127.01 (phenethyl C4); 127.17 (phenethyl C2, C6); 128.07 (phenethyl C3, C5, =CH-); 128.93 (benzohydrazide C2, C6); 129.00 (benzohydrazide C3, C5); 129.23 (arylidene C5); 129.73 (arylidene C6); 130.80 (arylidene C4); 131.36 (arylidene C2); 132.21 (benzohydrazide C4); 133.64 (benzohydrazide C1); 135.36 (arylidene C1); 138.46 (phenethyl C1); 139.12 (arylidene C3); 156.58 (thiazolidinone C2); 163.99 (exocyclic C=O); 165.52 (endocyclic C=O). MS (APCI $^-$) m/z calculated for $C_{26}H_{23}N_3O_2S$ $[M-H]^-$, 440.14; found 440.25.

N'-[5-(2,5-Dimethoxybenzylidene)-3-propyl-4-oxo-1,3-thiazolidin-2-ylidene]isonicotinohydrazide (9)

Orange powder. M.p. 178-180 °C. Elemental analysis calculated for $C_{21}H_{22}N_4O_4S \cdot 1/3H_2O$: C 58.32, H 5.28, N 12.95, S 7.41; found: C 58.61, H 5.328, N 12.95, S 7.228. IR (cm^{-1}): 3109 (N-H); 1697 (C=O). 1H NMR δ ppm (400 MHz, DMSO- d_6 , TMS): 0.92 (t, 3H, $J_1 = 7.24$ Hz, $J_2 = 7.32$ Hz, CH_2-CH_3); 1.75 (q, 2H, CH_2-CH_3); 3.73 (s, 3H, Ar-(5) OCH_3); 3.86 (t, 5H, Ar-(2) OCH_3 and N- CH_2-CH_2); 6.96 (s, 1H, arylidene H4); 7.09 (s, 2H, arylidene H3, H6); 7.78 (d, 2H, $J = 4.56$ Hz, pyridine H3, H5); 7.89 (s, 1H, =CH-Ar); 8.77 (d, 2H, $J = 4.6$ Hz, pyridine H2, H6); 11.48 (s, 1H, NH-N). ^{13}C NMR (100 MHz) (DMSO- d_6 /TMS) δ ppm: 11.54 ($-CH_2-CH_3$); 20.52 ($-CH_2-CH_2-CH_3$); 44.90 (N- CH_2-CH_2-); 55.98 ($-OCH_3(5)$); 56.55 ($-OCH_3(2)$); 113.33 (arylidene C4); 114.64 (arylidene C6); 116.90 (arylidene C3); 121.75 (arylidene C1); 121.87 (pyridine C3, C5); 122.82 (thiazolidinone C5); 125.46 (=CH-); 140.69 (pyridine C4); 150.79 (pyridine C2, C6); 152.59 (arylidene C2); 153.45 (arylidene C5); 156.73 (thiazolidinone C2); 162.22 (exocyclic C=O); 165.90 (endocyclic C=O). MS (APCI $^+$) m/z calculated for $C_{21}H_{22}N_4O_4S$ $[M+H]^+$, 427.14; found 427.25.

N'-[5-(2-Methoxybenzylidene)-3-allyl-4-oxo-1,3-thiazolidin-2-ylidene]isonicotinohydrazide (10)

Beige powder. M.p. 216-217 °C. Elemental analysis calculated for $C_{20}H_{18}N_4O_3S \cdot 1/3H_2O$: C 59.99, H 4.70, N 13.99, S 8.01; found: C 60.06, H 4.559, N 13.95, S 7.908. IR (cm^{-1}): 3209 (N-H); 1701, 1654 (C=O). 1H NMR δ ppm (400 MHz, DMSO- d_6 , TMS): 3.89 (s, 3H, Ar- OCH_3); 4.52 (s, 2H, N- CH_2-CH); 5.22 (d, 2H, $J = 12$ Hz, $-CH=CH_2$); 5.96 (m, 1H, $CH_2-CH=CH_2$); 7.08 – 7.97 (m, 7H, Ar-H, pyridine H3, H5, =CH-Ar); 8.77 (d, 2H, $J = 3.2$ Hz, pyridine H2, H6); 11.51 (s, 1H, NH-

N). ^{13}C NMR (100 MHz) (DMSO- d_6 /TMS) δ ppm: 46.26 (>N-CH $_2$ -); 56.26 (-O-CH $_3$); 112.31 (arylidene C3); 117.95 (=CH $_2$); 120.90 (arylidene C5); 121.46 (arylidene C1); 121.88 (arylidene C4); 122.06 (pyridine C3, C5); 125.71 (thiazolidinone C5); 129.06 (=CH-); 131.47 (arylidene C6); 132.69 (-CH=CH $_2$); 140.45 (pyridine C4); 150.81 (pyridine C2, C6); 157.08 (thiazolidinone C2); 158.34 (arylidene C2); 162.21 (exocyclic C=O); 165.65 (endocyclic C=O). MS (APCI $^+$) m/z calculated for C $_{20}$ H $_{18}$ N $_4$ O $_3$ S [M-H] $^+$, 393.10; found 393.20.

N'-[5-(2-Chloro-6-fluorobenzylidene)-3-allyl-4-oxo-1,3-thiazolidin-2-ylidene]isonicotinohydrazide (11)

Yellow powder. M.p. 150-153 °C. Elemental analysis calculated for C $_{19}$ H $_{14}$ ClFN $_4$ O $_2$ S.1/3C $_2$ H $_5$ OH: C 54.65, H 3.73, N 12.96, S 7.42; found: C 54.44, H 4.140, N 13.27, S 7.596. IR (cm $^{-1}$): 3086 (N-H); 1705 (C=O). ^1H NMR δ ppm (400 MHz, DMSO- d_6 , TMS): 4.53 (s, 2H, N-CH $_2$ -CH-); 5.26 (t, 2H, -CH=CH $_2$); 5.96 (m, 1H, CH $_2$ -CH=CH $_2$); 7.37 – 7.74 (m, 8H, Ar-H, pyridine H3, H5, =CH-Ar); 8.73 (d, 2H, J=4.52 Hz, pyridine H2, H6); 11.52 (s, 1H, NH-N). ^{13}C NMR (100 MHz) (DMSO- d_6 /TMS) δ ppm: 45.61 (>N-CH $_2$ -); 115.72-115.94 (arylidene C5); 118.31 (=CH $_2$); 120.82-121.00 (arylidene C1); 121.82 (pyridine C3, C5); 122.45 (thiazolidinone C5); 126.56 (arylidene C3); 126.59 (=CH-); 129.17 (-CH=CH $_2$); 131.35-131.93 (arylidene C4); 133.02 (arylidene C2); 140.31 (pyridine C4); 150.77 (pyridine C2, C6); 155.59 (thiazolidinone C2); 158.19-160.69 (arylidene C6); 162.08 (exocyclic C=O); 164.39 (endocyclic C=O). MS (APCI $^+$) m/z calculated for C $_{19}$ H $_{14}$ ClFN $_4$ O $_2$ S [M-H] $^+$, 415.04; found 415.15.

N'-[5-(2-Chlorobenzylidene)-3-benzyl-4-oxo-1,3-thiazolidin-2-ylidene]isonicotinohydrazide (12)

Yellow powder. M.p. 210-212 °C. Elemental analysis calculated for C $_{23}$ H $_{17}$ ClN $_4$ O $_2$ S: C 61.54, H 3.82, N 12.48, S 7.14; found: C 61.30; H 3.810; N 12.42; S 6.962. IR (cm $^{-1}$): 3062 (N-H); 1697 (C=O). ^1H NMR δ ppm (400 MHz, DMSO- d_6 , TMS): 5.12 (s, 2H, CH $_2$ -Ar); 7.33 (m, 11H, Ar-H, pyridine H3, H5); 7.95 (s, 1H, =CH-Ar); 8.77 (d, 2H, J=4.04 Hz, pyridine H2, H6); 11.59 (s, 1H, NH-N). ^{13}C NMR (100 MHz) (DMSO- d_6 /TMS) δ ppm: 46.62 (-CH $_2$ -); 121.92 (pyridine C3, C5); 124.61 (thiazolidinone C5); 126.37 (=CH-); 128.27 (benzyl C4); 128.42 (benzyl C2, C6); 128.66 (arylidene C5); 129.07 (benzyl C3, C5); 129.53 (arylidene C3); 130.84 (arylidene C6); 131.58 (arylidene C4); 132.19 (arylidene C1); 134.71 (arylidene C2); 136.08 (benzyl C1); 140.25 (pyridine C4); 150.82 (pyridine C2, C6); 156.54 (thiazolidinone C2); 162.10 (exocyclic C=O); 165.50 (endocyclic C=O). MS (APCI $^+$) m/z calculated for C $_{23}$ H $_{17}$ ClN $_4$ O $_2$ S [M-H] $^+$, 447.07; found 447.15.

N'-[5-(2-Methoxybenzylidene)-3-benzyl-4-oxo-1,3-thiazolidin-2-ylidene]isonicotinohydrazide (13)

Yellow powder. M.p. 224-225 °C. Elemental analysis calculated for C $_{24}$ H $_{20}$ N $_4$ O $_3$ S.2H $_2$ O: C 59.99, H 5.03, N 11.66, S 6.67; found: C 59.62, H 4.764, N 11.49, S 6.453. IR (cm $^{-1}$): 3151 (N-H); 1697 (C=O). ^1H NMR δ ppm (400 MHz, DMSO- d_6 , TMS): 3.89 (s, 3H, Ar-OCH $_3$); 5.09 (s, 2H, CH $_2$ -Ar); 7.12-7.52 (m, 9H, Ar-H); 7.82 (d, 2H, J=5.64 Hz, pyridine H3, H5); 7.89 (s, 1H, =CH-Ar); 8.64 (d, 2H, J=4.48 Hz, pyridine H2, H6); (N-H proton was exchanged with DMSO deuterium.). ^{13}C NMR (100 MHz) (DMSO- d_6 /TMS) δ ppm: 46.18 (-CH $_2$ -); 56.19 (-O-CH $_3$); 112.09 (arylidene C3); 121.33 (pyridine C3, C5); 122.23 (arylidene C5); 122.77 (arylidene C1); 122.84 (arylidene C4); 123.18 (thiazolidinone C5); 127.90 (=CH-); 128.19 (benzyl C4); 128.82 (benzyl C2, C6); 128.87 (benzyl C3, C5); 131.90 (arylidene C6); 136.82 (benzyl C1); 145.17 (pyridine C4); 149.28 (pyridine C2, C6); 149.99 (thiazolidinone C2); 158.15 (arylidene C2);

163.43 (exocyclic C=O); 166.35 (endocyclic C=O). MS (APCI⁻) m/z calculated for C₂₄H₂₀N₄O₃S [M-H]⁻, 443.11; found 443.20.

N'-[5-(3-Chlorobenzylidene)-3-benzyl-4-oxo-1,3-thiazolidin-2-ylidene]isonicotinohydrazide (14)

Yellow powder. M.p. 214-215 °C. Elemental analysis calculated for C₂₃H₁₇ClN₄O₂S: C 61.79, H 4.56, N 11.53, S 6.60; found: C 62.11, H 4.522, N 11.78, S 6.553. IR (cm⁻¹): 3186 (N-H); 1705 (C=O). ¹H NMR δ ppm (400 MHz, DMSO- d₆, TMS): 5.12 (s, 2H, -CH₂-Ar); 7.27-7.68 (m, 10H, Ar-H, =CH-Ar); 7.86 (d, J=5.6 Hz, pyridine H3, H5); 8.51 (d, 2H, J=5.56 Hz, pyridine H2, H6); (N-H proton was exchanged with DMSO deuterium). ¹³C NMR (100 MHz) (DMSO-d₆/TMS) δ ppm: 46.19 (-CH₂-); 122.43 (pyridine C3, C5); 125.37 (thiazolidinone C5); 126.33 (=CH-); 127.75 (benzyl C4); 127.93 (benzyl C2, C6); 128.10 (benzyl C3, C5); 128.81 (arylidene C6); 129.09 (arylidene C5); 129.99 (arylidene C2); 134.17 (arylidene C4); 134.17 (arylidene C3); 136.97 (arylidene C1); 137.23 (benzyl C1); 143.58 (pyridine C4); 148.77 (pyridine C2, C6); 149.49 (thiazolidinone C2); 164.95 (exocyclic C=O); 166.38 (endocyclic C=O). MS (APCI⁻) m/z calculated for C₂₃H₁₇ClN₄O₂S [M-H]⁻, 447.07; found 447.15.

N'-[5-(3-Methoxybenzylidene)-3-benzyl-4-oxo-1,3-thiazolidin-2-ylidene]isonicotinohydrazide (15)

Yellow powder. M.p. 190-193 °C. Elemental analysis calculated for C₂₄H₂₀N₄O₃S.1/3C₂H₅OH: C 64.42, H 4.82, N 12.18, S 6.97; found: C 64.47, H 5.021, N 12.59, S 7.234. IR (cm⁻¹): 3074 (N-H); 1701 (C=O). ¹H NMR δ ppm (400 MHz, DMSO- d₆, TMS): 3.80 (s, 3H, Ar-OCH₃); 5.12 (s, 2H, -CH₂-Ar); 7.06-7.80 (m, 12H, Ar-H, pyridine H3, H5, =CH-Ar); 8.77 (s, 2H, pyridine H2, H6), 11.57 (1H, s, NH-N). ¹³C NMR (100 MHz) (DMSO-d₆/TMS) δ ppm: 46.45 (-CH₂-); 55.76 (-O-CH₃); 116.27 (arylidene C4); 116.42 (arylidene C2); 121.34 (arylidene C6); 121.91 (pyridine C3, C5); 121.99 (thiazolidinone C5); 128.20 (=CH-); 128.31 (benzyl C4); 129.04 (benzyl C2, C6); 130.96 (benzyl C3, C5); 131.32 (arylidene C5); 135.01 (arylidene C1); 136.21 (benzyl C1); 140.47 (pyridine C4); 150.80 (pyridine C2, C6); 156.38 (thiazolidinone C2); 160.08 (arylidene C3); 162.14 (exocyclic C=O); 165.83 (endocyclic C=O). MS (APCI⁺) m/z calculated for C₂₄H₂₀N₄O₃S [M+H]⁺, 445.14; found 445.20.

N'-[5-(2,5-Dimethoxybenzylidene)-3-benzyl-4-oxo-1,3-thiazolidin-2-ylidene]isonicotinohydrazide (16)

Yellow powder. M.p. 82-84 °C. Elemental analysis calculated for C₂₅H₂₂N₄O₄S.5/2H₂O: C 57.79, H 5.24, N 10.78, S 6.17; found: C 57.98, H 4.789, N 10.83, S 5.971. IR (cm⁻¹): 3078 (N-H); 1697 (C=O). ¹H NMR δ ppm (400 MHz, DMSO- d₆, TMS): 3.73 (s, 3H, -O-CH₃(5)); 3.79 (s, 3H, -O-CH₃(2)); 5.10 (s, 2H, CH₂-Ar); 6.97 (s, 1H, arylidene H6); 7.09 (s, 2H, arylidene H3-H4); 7.31-7.45 (m, 5H, Ar-H); 7.79 (d, 2H, J=4.24 Hz, pyridine H3, H5); 7.92 (s, 1H, =CH-Ar); 8.77 (d, 2H, J=4.76 Hz, pyridine H2, H6); 11.54 (s, 1H, NH-N). ¹³C NMR δ ppm (APT, DMSO-d₆, 125 MHz, TMS): 46.40 (-CH₂-); 56.02 (-O-CH₃(5)); 56.59 (-O-CH₃(2)); 113.43 (arylidene C4); 114.73 (arylidene C6); 117.14 (arylidene C3); 121.55 (arylidene C1); 121.87 (pyridine C3, C5); 122.75 (thiazolidinone C5); 126.09 (=CH-); 128.19 (benzyl C4); 128.35 (benzyl C2, C6); 129.02 (benzyl C3, C5); 136.22 (benzyl C1); 140.47 (pyridine C4); 150.80 (pyridine C2, C6); 152.63 (arylidene C2); 153.49 (arylidene C5); 156.32 (thiazolidinone C2); 165.82 (endocyclic C=O). 2D ¹H-¹³C HSQC δ ppm (DMSO- d₆, TMS): 3.73 - 56.03 (-O-CH₃(5)); 3.83 - 56.60 (-O-CH₃(2)); 5.10 - 46.41 (-CH₂-); 6.96 - 114.76 (arylidene H6-C6); 7.08 - 113.47 (arylidene H4-C4); 7.08 - 117.19 (arylidene H3-C3); 7.30 - 128.20 (benzyl H4-C4); 7.37 - 129.03 (benzyl H3-C3, H5-C5); 7.45 - 128.44 (benzyl H2-C2, H6-C6); 7.79 - 121.91 (pyridine H3-C3, H5-C5); 7.93 - 126.10

(=CH-); 8.76 - 150.70 (pyridine H2-C2, H6-C6). 2D ^1H - ^{13}C HMBC δ ppm (DMSO- d_6 , TMS): 5.10 (128.38, 136.20, 156.29, 165.79); 7.80 (150.75, 162.53); 7.91 (165.81). MS (APCI $^-$) m/z calculated for $\text{C}_{25}\text{H}_{22}\text{N}_4\text{O}_4\text{S}$ $[\text{M}-\text{H}]^-$, 473.13; found 473.25.

N'-[5-(2,5-Dimethoxybenzylidene)-3-phenethyl-4-oxo-1,3-thiazolidin-2-ylidene]isonicotinohydrazide (17)

Yellow powder. M.p. 195-200 °C. Elemental analysis calculated for $\text{C}_{26}\text{H}_{24}\text{N}_4\text{O}_4\text{S}$: C 63.92, H 4.95, N 11.47, S 6.56; found: C 63.93, H 5.058, N 11.96, S 6.753. IR (cm^{-1}): 3213 (N-H); 1712, 1651 (C=O). ^1H NMR δ ppm (400 MHz, DMSO- d_6 , TMS): 3.07 (s, 2H, CH_2 -Ar); 3.74 (s, 3H, Ar-(5) OCH_3); 3.83 (s, 3H, Ar-(2) OCH_3); 4.12 (s, 2H, N- CH_2); 6.95 (s, 1H, arylidene H4); 7.09 (s, 2H, arylidene H3-H6); 7.23-7.31 (d, 5H, Ar-H); 7.82 (d, 3H, pyridine H3, H5, =CH-Ar); 8.79 (s, 2H, pyridine H2, H6); 11.57 (s, 1H, NH-N). ^{13}C NMR (100 MHz) (DMSO- d_6 /TMS) δ ppm: 32.67 (- CH_2 -Ar); 44.50 (>N- CH_2 -); 56.00 (- OCH_3 (5)); 56.56 (- OCH_3 (2)); 113.38 (arylidene C4); 114.62 (arylidene C6); 116.99 (arylidene C3); 121.93 (pyridine C3, C5; arylidene C1); 122.70 (thiazolidinone C5); 125.49 (=CH-); 127.01 (phenethyl C4); 128.94 (phenethyl C2, C6); 129.21 (phenethyl C3, C5); 138.43 (phenethyl C1); 140.56 (pyridine C4); 150.84 (pyridine C2, C6); 152.60 (arylidene C2); 153.45 (arylidene C5); 156.46 (thiazolidinone C2); 162.63 (exocyclic C=O); 165.48 (endocyclic C=O). MS (APCI $^-$) m/z calculated for $\text{C}_{26}\text{H}_{24}\text{N}_4\text{O}_4\text{S}$ $[\text{M}-\text{H}]^-$, 487.14; found 487.20.

N'-[5-(2-Methoxybenzylidene)-3-propyl-4-oxo-1,3-thiazolidin-2-ylidene]nicotinohydrazide (18)

Light yellow powder. M.p. 222-223 °C. Elemental analysis calculated for $\text{C}_{20}\text{H}_{20}\text{N}_4\text{O}_3\text{S}$: C 60.59, H 5.08, N 14.13, S 8.09; found: C 60.17, H 5.139, N 14.09, S 7.981. IR (cm^{-1}): 3190 (N-H); 1697, 1643 (C=O). ^1H NMR δ ppm (400 MHz, DMSO- d_6 , TMS): 0.93 (t, 3H, - CH_2 - CH_2 - CH_3); 1.75 (m, 2H, - CH_2 - CH_2 - CH_3); 3.90 (d, 5H, Ar- OCH_3 , N- CH_2 - CH_2); 7.10-7.58 (m, 5H, Ar-H, =CH-Ar); 7.97 (s, 1H, pyridine H5); 8.23 (d, 1H, $J=3.6$ Hz, pyridine H4); 8.77 (s, 1H, pyridine H6); 9.04 (s, 1H, pyridine H2); 11.39 (1H, s, NH-N). ^{13}C NMR (100 MHz) (DMSO- d_6 /TMS) δ ppm: 11.56 (- CH_2 - CH_3); 20.53 (- CH_2 - CH_2 - CH_3); 44.91 (N- CH_2 - CH_2 -); 56.28 (-O- CH_3); 112.33 (arylidene C3); 121.10 (arylidene C5); 121.48 (arylidene C1); 122.14 (arylidene C4); 124.12 (pyridine C5); 125.41 (thiazolidinone C5); 129.05 (=CH-); 132.61 (pyridine C3); 135.75 (arylidene C6); 136.95 (pyridine C4); 148.93 (pyridine C2); 152.69 (pyridine C6); 158.32 (arylidene C2, thiazolidinone C2); 162.58 (exocyclic C=O); 166.07 (endocyclic C=O). MS (APCI $^-$) m/z calculated for $\text{C}_{20}\text{H}_{20}\text{N}_4\text{O}_3\text{S}$ $[\text{M}-\text{H}]^-$, 395.12; found 395.20.

N'-[5-(3-Methoxybenzylidene)-3-propyl-4-oxo-1,3-thiazolidin-2-ylidene]nicotinohydrazide (19)

Light yellow powder. M.p. 175-177 °C. Elemental analysis calculated for $\text{C}_{20}\text{H}_{20}\text{N}_4\text{O}_3\text{S}$: C 60.59, H 5.08, N 14.13, S 8.09; found: C 60.57, H 5.321, N 13.99, S 8.123. IR (cm^{-1}): 3201 (N-H); 1697 (C=O). ^1H NMR δ ppm (400 MHz, DMSO- d_6 , TMS): 0.93 (t, 3H, $J_1=6.64$ Hz, $J_2=6.88$ Hz, - CH_2 - CH_2 - CH_3); 1.76 (d, 2H, $J=6.84$ Hz, - CH_2 - CH_2 - CH_3); 3.84 (d, 5H, Ar- OCH_3 , N- CH_2 - CH_2); 7.05-7.58 (m, 5H, Ar-H, =CH-Ar); 7.76 (s, 1H, pyridine H5); 8.24 (d, 1H, $J=6.88$ Hz, pyridine H4); 8.78 (s, 1H, pyridine H6); 9.05 (s, 1H, pyridine H2); 11.42 (1H, s, NH-N). ^{13}C NMR (100 MHz) (DMSO- d_6 /TMS) δ ppm: 11.55 (- CH_2 - CH_3); 20.52 (- CH_2 - CH_2 - CH_3); 44.96 (N- CH_2 - CH_2 -); 55.73 (-O- CH_3); 116.17 (arylidene C4); 116.38 (arylidene C2); 121.51 (arylidene C6); 121.97 (thiazolidinone C5); 124.12 (pyridine C5); 129.31 (=CH-); 130.83 (pyridine C3); 130.93 (arylidene C5); 135.07 (arylidene C1); 135.80 (pyridine C4); 148.96 (pyridine C2); 152.71 (pyridine C6); 156.77 (thiazolidinone C2); 160.07 (arylidene C3); 162.70 (exocyclic C=O);

168.88 (endocyclic C=O). MS (APCI⁻) m/z calculated for C₂₀H₂₀N₄O₃S [M-H]⁻, 395.12; found 395.20.

N'-[5-(2-Methoxybenzylidene)-3-benzyl-4-oxo-1,3-thiazolidin-2-ylidene]nicotinohydrazide (20)

Light yellow powder. M.p. 193-195 °C. Elemental analysis calculated for C₂₄H₂₀N₄O₃S.H₂O: C 62.32, H 4.79, N 12.11, S 6.93; found: C 62.29, H 4.845, N 12.17, S 6.906. IR (cm⁻¹): 3209 (N-H); 1705 (C=O). ¹H NMR δ ppm (400 MHz, DMSO- d₆, TMS): 3.90 (s, 3H, Ar-OCH₃); 5.10 (s, 2H, N-CH₂); 7.09-7.58 (m, 10H, Ar-H, =CH-Ar); 8.00 (s, 1H, pyridine H5); 8.23 (d, 1H, J=6.84 Hz, pyridine H4); 8.76 (d, 1H, J=3.04 Hz, pyridine H6); 9.04 (s, 1H, pyridine H2); 11.43 (1H, s, NH-N). ¹³C NMR (100 MHz) (DMSO-d₆/TMS) δ ppm: 46.40 (-CH₂-); 56.28 (-O-CH₃); 112.34 (arylidene C3); 120.87 (arylidene C5); 121.49 (arylidene C1); 122.06 (arylidene C4); 124.10 (pyridine C5); 125.89 (thiazolidinone C5); 128.19 (=CH-); 128.33 (benzyl C4); 129.04 (benzyl C2, C6); 129.12 (benzyl C3, C5); 130.59 (pyridine C3); 132.74 (arylidene C6); 135.80 (pyridine C4); 136.25 (benzyl C1); 148.97 (pyridine C2); 152.71 (pyridine C6); 156.70 (thiazolidinone C2); 158.35 (arylidene C2); 162.57 (exocyclic C=O); 166.00 (endocyclic C=O). MS (APCI⁻) m/z calculated for C₂₄H₂₀N₄O₃S [M-H]⁻, 443.12 found 443.20.

N'-[5-(3-Chlorobenzylidene)-3-benzyl-4-oxo-1,3-thiazolidin-2-ylidene]nicotinohydrazide (21)

Light yellow powder. M.p. 208-211 °C. Elemental analysis calculated for C₂₃H₁₇ClN₄O₂S.1/3H₂O: C 60.72, H 3.91, N 12.32, S 7.05; found: C 60.88, H 3.609, N 12.35, S 6.865. IR (cm⁻¹): 3066 (N-H); 1716 (C=O). ¹H NMR δ ppm (400 MHz, DMSO- d₆, TMS): 5.12 (s, 2H, N-CH₂-Ar); 7.31-7.81 (m, 11H, Ar-H, =CH-Ar, pyridine H5); 8.24 (d, 1H, J=6.80 Hz, pyridine H4); 8.76 (d, 1H, J=2.92 Hz, pyridine H6); 9.06 (s, 1H, pyridine H2); 11.49 (1H, s, NH-N). ¹³C NMR (100 MHz) (DMSO-d₆/TMS) δ ppm: 45.54 (-CH₂-); 122.78 (thiazolidinone C5); 124.09 (pyridine C5); 128.14 (=CH-); 128.15 (benzyl C4); 128.23 (benzyl C2, C6); 128.39 (benzyl C3, C5); 129.04 (arylidene C6); 129.65 (pyridine C3); 130.28 (arylidene C5); 130.45 (arylidene C2); 131.62 (arylidene C4); 134.40 (arylidene C3); 135.83 (pyridine C4, arylidene C1); 136.15 (benzyl C1); 149.04 (pyridine C2); 152.74 (pyridine C6); 155.37 (thiazolidinone C2); 162.70 (exocyclic C=O); 165.63 (endocyclic C=O). MS (APCI⁻) m/z calculated for C₂₃H₁₇ClN₄O₂S [M-H]⁻, 447.07; found 447.15.

N'-[5-(2-Bromobenzylidene)-3-phenethyl-4-oxo-1,3-thiazolidin-2-ylidene]nicotinohydrazide (22)

Light yellow powder. M.p. 184-186 °C. Elemental analysis calculated for C₂₄H₁₉BrN₄O₂S.1/2H₂O: C 55.82, H 3.90, N 10.85, S 6.21; found: C 56.18, H 3.655, N 11.01, S 6.033. IR (cm⁻¹): 3201 (N-H); 1708 (C=O). ¹H NMR δ ppm (400 MHz, DMSO- d₆, TMS): 3.10 (s, 2H, CH₂-Ar); 4.13 (s, 2H, N-CH₂); 7.24-7.82 (m, 11H, Ar-H, =CH-Ar, pyridine H5); 8.25 (d, 1H, J=7.2 Hz, pyridine H4); 8.77 (d, 1H, pyridine H6); 9.07 (s, 1H, pyridine H2); 11.52 (1H, s, NH-N). ¹³C NMR (100 MHz) (DMSO-d₆/TMS) δ ppm: 32.67 (-CH₂-Ar); 44.69 (>N-CH₂-); 124.70 (pyridine C5); 124.77 (thiazolidinone C5); 125.55 (arylidene C2); 127.04 (phenethyl C4); 128.65 (phenethyl C2, C6); 128.97 (arylidene C5); 129.11 (pyridine C3); 129.20 (phenethyl C3, C5); 129.21 (=CH-); 129.52 (arylidene C6); 132.19 (arylidene C4); 133.32 (arylidene C3); 134.07 (arylidene C1); 135.87 (pyridine C4); 138.39 (phenethyl C1); 149.05 (pyridine C2); 152.77 (pyridine C6); 156.14 (thiazolidinone C2); 162.79 (exocyclic C=O); 165.02 (endocyclic C=O). MS (APCI⁺) m/z calculated for C₂₄H₁₉BrN₄O₂S [M+Na]⁺, 529.02 found 529.10.

N'-[5-(2-Methoxybenzylidene)-3-phenethyl-4-oxo-1,3-thiazolidin-2-ylidene]nicotinohydrazide (23)

Light yellow powder. M.p. 181-182 °C. Elemental analysis calculated for $C_{25}H_{22}N_4O_3S \cdot 1/3H_2O$: C 64.64, H 4.92, N 12.06, S 6.90; found: C 64.91, H 4.645, N 12.17, S 6.518. IR (cm^{-1}): 3116 (N-H); 1651 (C=O). 1H NMR δ ppm (400 MHz, DMSO- d_6 , TMS): 3.09 (s, 2H, CH_2 -Ar); 3.89 (s, 3H, Ar- OCH_3); 4.12 (s, 2H, N- CH_2); 7.09-7.58 (m, 10H, Ar-H, =CH-Ar); 7.88 (s, 1H, pyridine H5); 8.26 (d, 1H, J=7.36 Hz, pyridine H4); 8.78 (d, 1H, J=3.64 Hz, pyridine H6); 9.08 (s, 1H, pyridine H2); 11.47 (1H, s, NH-N). ^{13}C NMR (100 MHz) (DMSO- d_6 /TMS) δ ppm: 32.64 (- CH_2 -Ar); 44.51 (>N- CH_2 -); 56.27 (-O- CH_3); 112.33 (arylidene C3); 120.86 (arylidene C5); 121.47 (arylidene C1); 122.03 (arylidene C4); 124.13 (pyridine C5); 125.37 (thiazolidinone C5); 127.01 (phenethyl C4); 128.94 (phenethyl C2, C6); 129.03 (=CH-); 129.21 (pyridine C3); 129.22 (phenethyl C3, C5); 132.64 (arylidene C6); 135.85 (phenethyl C4); 138.45 (phenethyl C1); 149.02 (pyridine C2); 152.74 (pyridine C6); 156.98 (thiazolidinone C2); 158.31 (arylidene C2); 162.75 (exocyclic C=O); 165.61 (endocyclic C=O). MS (APCI $^+$) m/z calculated for $C_{25}H_{22}N_4O_3S$ [M-H] $^+$, 457.13; found 457.25.

3.3 *In vitro* studies

3.3.1 Antimycobacterial activity

Briefly, the inoculum was prepared from fresh LJ medium re-suspended in 7H9-S medium (7H9 broth, 0.1% casitone, 0.5% glycerol, supplemented oleic acid, albumin, dextrose, and catalase [OADC]), adjusted to a OD_{590} 1.0, and diluted 1:20; 100 μ l was used as inoculum. Each drug stock solution was thawed and diluted in 7H9-S at four-fold the final highest concentration tested. Serial two-fold dilutions of each drug were prepared directly in a sterile 96-well microtiter plate using 100 μ l 7H9-S. A growth control containing no antibiotic and a sterile control were also prepared on each plate. Sterile water was added to all perimeter wells to avoid evaporation during the incubation. The plate was covered, sealed in plastic bags and incubated at 37°C in normal atmosphere. After 7 days incubation, 30 μ l of alamar blue solution was added to each well, and the plate was re-incubated overnight. A change in colour from blue (oxidised state) to pink (reduced) indicated the growth of bacteria, and the MIC was defined as the lowest concentration of drug that prevented this change in colour.

3.3.2 *MtInhA* inhibition assay μ M

4. CONCLUSION

Molecular modelling studies of an in house database of ~2200 compounds against five different *MtInhA* cocrystal structures, with and without NADH, were performed and twenty three 2-acylhydrazono-5-arylmethylene-4-thiazolidinone were selected for synthesis. After structural evaluation of the compounds, the *in vitro* antimycobacterial activities of all compounds were examined. The strongest mycobacterial growth inhibition (MIC: 6.25 μ g/mL) is observed for compounds **12** and **22**, however these compounds only showed weak inhibition of *MtInhA* at 50 μ M. Interestingly, compound **3** showed a higher MIC value (>6.25 μ g/mL) and the strongest measured *MtInhA* inhibition (51% at 50 μ M). The results indicate that potentially new scaffolds have been obtained for the investigation of antimycobacterial compounds.

Funding

This study was carried out without any funding.

Acknowledgement

Serap İpek Dingiş Birgül was supported with scholarships by the Council of Higher Education (CoHE) and The Scientific and Technological Research Council of Turkey (TUBITAK).

Abbreviations (dergi istiyorsa eklenecek)

MtInhA:

TB: Tuberculosis

WHO: World Health Organization

HMBC: Heteronuclear multiple bond correlation

HSQC: Heteronuclear single quantum coherence

NMR: Nuclear magnetic resonance spectroscopy

IR: Infrared spectroscopy

MS: Mass spectrometry

MIC: Minimum inhibitory concentration

MD: Molecular dynamics

ADME: Absorption, distribution, metabolism, and excretion

PDB: Protein Data Bank

MM-GBSA: Molecular modeling - generalised Born and surface area solvation

Appendix

The following are the Supplementary data to this article:

Supplementary data-1

REFERENCES

- (1) Islam, M. M.; Hameed, H. M. A.; Mugweru, J.; Chhotaray, C.; Wang, C. W.; Tan, Y. J.; Liu, J. X.; Li, X. J.; Tan, S. Y.; Ojima, I.; et al. Drug resistance mechanisms and novel drug targets for tuberculosis therapy. *J Genet Genomics* **2017**, *44* (1), 21-37. DOI: 10.1016/j.jgg.2016.10.002.
- (2) Bhat, Z. S.; Rather, M. A.; Maqbool, M.; Ahmad, Z. Drug targets exploited in Mycobacterium tuberculosis: Pitfalls and promises on the horizon. *Biomed Pharmacother* **2018**, *103*, 1733-1747. DOI: 10.1016/j.biopha.2018.04.176.
- (3) (WHO), W. H. O. *Global Tuberculosis Report*. 2022. <https://www.who.int/teams/global-tuberculosis-programme/tb-reports/global-tuberculosis-report-2022> (accessed).
- (4) Gordon, S. V.; Parish, T. Microbe Profile: Mycobacterium tuberculosis: Humanity's deadly microbial foe. *Microbiol-Sgm* **2018**, *164* (4), 437-439. DOI: 10.1099/mic.0.000601.
- (5) Brennan, P. J. Structure, function, and biogenesis of the cell wall of Mycobacterium tuberculosis. *Tuberculosis* **2003**, *83* (1-3), 91-97. DOI: 10.1016/S1472-9792(02)00089-6. Bhat, Z. S.; Rather, M. A.; Maqbool, M.; UL Lah, H.; Yousuf, S. K.; Ahmad, Z. Cell wall: A versatile fountain of drug targets in

Mycobacterium tuberculosis. *Biomed Pharmacother* **2017**, *95*, 1520-1534. DOI:

10.1016/j.biopha.2017.09.036.

(6) Rozman, K.; Sosic, I.; Fernandez, R.; Young, R. J.; Mendoza, A.; Gobec, S.; Encinas, L. A new 'golden age' for the antitubercular target inhA. *Drug Discov Today* **2017**, *22* (3), 492-502. DOI:

10.1016/j.drudis.2016.09.009.

(7) Chetty, S.; Ramesh, M.; Singh-Pillay, A.; Soliman, M. E. S. Recent advancements in the development of anti-tuberculosis drugs. *Bioorganic & Medicinal Chemistry Letters* **2017**, *27* (3), 370-386. DOI: 10.1016/j.bmcl.2016.11.084.

(8) Campanico, A.; Moreira, R.; Lopes, F. Drug discovery in tuberculosis. New drug targets and antimycobacterial agents. *European Journal of Medicinal Chemistry* **2018**, *150*, 525-545. DOI: 10.1016/j.ejmech.2018.03.020.

(9) Sink, R.; Sosic, I.; Zivec, M.; Fernandez-Menendez, R.; Turk, S.; Pajk, S.; Alvarez-Gomez, D.; Lopez-Roman, E. M.; Gonzales-Cortez, C.; Rullas-Triconado, J.; et al. Design, Synthesis, and Evaluation of New Thiadiazole-Based Direct Inhibitors of Enoyl Acyl Carrier Protein Reductase (InhA) for the Treatment of Tuberculosis. *Journal of Medicinal Chemistry* **2015**, *58* (2), 613-624. DOI: 10.1021/jm501029r.

(10) Duan, X.; Xiang, X.; Xie, J. Crucial components of Mycobacterium type II fatty acid biosynthesis (Fas-II) and their inhibitors. *FEMS Microbiol Lett* **2014**, *360* (2), 87-99. DOI: 10.1111/1574-6968.12597 From NLM Medline.

(11) Tatar, E. K., İ.; Küçükgülzel, Ş.G.; Yılmaz-Demircan, F.; De Clercq, E.; Andrei, G.; Snoeck, R.; Pannecouque, C.; Şahin, F.; Bayrak, Ö.F. Synthesis, Anti-Tuberculosis and Antiviral Activity of Novel 2-isonicotinoylhydrazono-5-arylidene-4-thiazolidinones. *International Journal of Drug Design and Discovery* **2010**, *1* (1), 19-32.

(12) Tatar, E.; Kucukguzel, I.; De Clercq, E.; Krishnan, R.; Kaushik-Basu, N. Synthesis, characterization and antiviral evaluation of 1,3-Thiazolidine-4-one derivatives bearing L-Valine side chain. *Marmara Pharm J* **2012**, *16* (3), 181-193. DOI: 10.12991/201216397.

(13) Cakir, G.; Kucukguzel, I.; Guhamazumder, R.; Tatar, E.; Manvar, D.; Basu, A.; Patel, B. A.; Zia, J.; Talele, T. T.; Kaushik-Basu, N. Novel 4-Thiazolidinones as Non-Nucleoside Inhibitors of Hepatitis C Virus NS5B RNA-Dependent RNA Polymerase. *Arch Pharm* **2015**, *348* (1), 10-22. DOI: 10.1002/ardp.201400247.

(14) Manvar, D.; Kucukguzel, I.; Erensoy, G.; Tatar, E.; Deryabasogullari, G.; Reddy, H.; Talele, T. T.; Cevik, O.; Kaushik-Basu, N. Discovery of conjugated thiazolidinone-thiadiazole scaffold as anti-dengue virus polymerase inhibitors. *Biochem Bioph Res Co* **2016**, *469* (3), 743-747. DOI: 10.1016/j.bbrc.2015.12.042.

(15) Ture, A.; Ergul, M.; Ergul, M.; Altun, A.; Kucukguzel, I. Design, synthesis, and anticancer activity of novel 4-thiazolidinone-phenylaminopyrimidine hybrids. *Mol Divers* **2021**, *25* (2), 1025-1050. DOI: 10.1007/s11030-020-10087-1.

(16) Tatar, E.; Kucukguzel, I.; Otuk, G.; Bilgin, M.; De Clercq, E.; Andrei, G.; Snoeck, R.; Pannecouque, C.; Kaushik-Basu, N. Synthesis, characterization and biological evaluation of 1,3-thiazolidine-4-ones derived from (2S)-2-benzoylamino-3-methylbutanohydrazide hydrazones. *J Res Pharm* **2021**, *25* (4), 507-518. DOI: 10.29228/jrp.41.

(17) Kucukguzel, S. G.; Oruc, E. E.; Rollas, S.; Sahin, F.; Ozbek, A. Synthesis, characterisation and biological activity of novel 4-thiazolidinones, 1,3,4-oxadiazoles and some related compounds. *European Journal of Medicinal Chemistry* **2002**, *37* (3), 197-206. DOI: Pii S0223-5234(01)01326-5

Doi 10.1016/S0223-5234(01)01326-5.

(18) Poyraz, O.; Jeankumar, V. U.; Saxena, S.; Schnell, R.; Haraldsson, M.; Yogeeswari, P.; Sriram, D.; Schneider, G. Structure-Guided Design of Novel Thiazolidine Inhibitors of O-Acetyl Serine Sulphydrylase from Mycobacterium tuberculosis. *Journal of Medicinal Chemistry* **2013**, *56* (16), 6457-6466. DOI: 10.1021/jm400710k.

- (19) Devi, P. B.; Samala, G.; Sridevi, J. P.; Saxena, S.; Alvala, M.; Salina, E. G.; Sriram, D.; Yogeewari, P. Structure-Guided Design of Thiazolidine Derivatives as Mycobacterium tuberculosis Pantothenate Synthetase Inhibitors. *Chemmedchem* **2014**, *9* (11), 2538-2547. DOI: 10.1002/cmdc.201402171.
- (20) Slepikas, L.; Chiriano, G.; Perozzo, R.; Tardy, S.; Kranjc, A.; Patthey-Vuadens, O.; Ouertatani-Sakouhi, H.; Kicka, S.; Harrison, C. F.; Scignari, T.; et al. In Silico Driven Design and Synthesis of Rhodanine Derivatives as Novel Antibacterials Targeting the Enoyl Reductase InhA. *Journal of Medicinal Chemistry* **2016**, *59* (24), 10917-10928. DOI: 10.1021/acs.jmedchem.5b01620.
- (21) Berman, H. M.; Westbrook, J.; Feng, Z.; Gilliland, G.; Bhat, T. N.; Weissig, H.; Shindyalov, I. N.; Bourne, P. E. The Protein Data Bank. *Nucleic Acids Res* **2000**, *28* (1), 235-242. DOI: DOI 10.1093/nar/28.1.235.
- (22) Chollet, A.; Maveyraud, L.; Lherbet, C.; Bernardes-Genisson, V. An overview on crystal structures of InhA protein: Apo-form, in complex with its natural ligands and inhibitors. *Eur J Med Chem* **2018**, *146*, 318-343. DOI: 10.1016/j.ejmech.2018.01.047 From NLM Medline.
- (23) Lipinski, C. A.; Lombardo, F.; Dominy, B. W.; Feeney, P. J. Experimental and computational approaches to estimate solubility and permeability in drug discovery and development settings. *Adv Drug Deliver Rev* **2012**, *64*, 4-17. DOI: 10.1016/j.addr.2012.09.019.
- (24) Hamulakova, S.; Janovec, L.; Hrabanova, M.; Spilovska, K.; Korabecny, J.; Kristian, P.; Kuca, K.; Imrich, J. Synthesis and Biological Evaluation of Novel Tacrine Derivatives and Tacrine-Coumarin Hybrids as Cholinesterase Inhibitors. *Journal of Medicinal Chemistry* **2014**, *57* (16), 7073-7084. DOI: 10.1021/jm5008648.
- (25) Kucukguzel, I.; Satilmis, G.; Gurukumar, K. R.; Basu, A.; Tatar, E.; Nichols, D. B.; Talele, T. T.; Kaushik-Basu, N. 2-Heteroarylimino-5-arylidene-4-thiazolidinones as a new class of non-nucleoside inhibitors of HCV NS5B polymerase. *European Journal of Medicinal Chemistry* **2013**, *69*, 931-941. DOI: 10.1016/j.ejmech.2013.08.043.
- (26) Vicini, P.; Geronikaki, A.; Anastasia, K.; Incerti, M.; Zani, F. Synthesis and antimicrobial activity of novel 2-thiazolylimino-5-arylidene-4-thiazolidinones. *Bioorgan Med Chem* **2006**, *14* (11), 3859-3864. DOI: 10.1016/j.bmc.2006.01.043.
- (27) Petrou, A.; Zagaliotis, P.; Theodoroula, N. F.; Mystridis, G. A.; Vizirianakis, I. S.; Walsh, T. J.; Geronikaki, A. Thiazole/Thiadiazole/Benzothiazole Based Thiazolidin-4-One Derivatives as Potential Inhibitors of Main Protease of SARS-CoV-2. *Molecules* **2022**, *27* (7). DOI: ARTN 2180 10.3390/molecules27072180.
- (28) Rodrigues, D. A.; Guerra, F. S.; Sagrillo, F. S.; Pinheiro, P. D. M.; Alves, M. A.; Thota, S.; Chaves, L. S.; Sant'Anna, C. M. R.; Fernandes, P. D.; Fraga, C. A. M. Design, Synthesis, and Pharmacological Evaluation of First-in-Class Multitarget N-Acylhydrazone Derivatives as Selective HDAC6/8 and PI3K alpha Inhibitors. *Chemmedchem* **2020**, *15* (6), 539-551. DOI: 10.1002/cmdc.201900716.
- (29) Shehata, I. A.; Glennon, R. A. Mesoionic Isoxazolo[2,3-a]Pyrimidinediones and 1,3,4-Oxadiazolo[3,2-a]Pyrimidinediones as Potential Adenosine Antagonists. *Journal of Heterocyclic Chemistry* **1987**, *24* (5), 1291-1295. DOI: DOI 10.1002/jhet.5570240511.
- (30) Hordiichuk, O. R.; Kinzhybalo, V. V.; Goreshnik, E. A.; Slyvka, Y. I.; Krawczyk, M. S.; Mys'kiv, M. G. Influence of apical ligands on Cu-(C=C) interaction in Copper(I) halides (Cl-, Br-, I-) pi-complexes with an 1,2,4-triazole allyl-derivative: Syntheses, crystal structures and NMR spectroscopy. *J Organomet Chem* **2017**, *838*, 1-8. DOI: 10.1016/j.jorganchem.2017.03.022.
- (31) Yang, S. J.; Lee, S. H.; Kwak, H. J.; Gong, Y. D. Regioselective Synthesis of 2-Amino-Substituted 1,3,4-Oxadiazole and 1,3,4-Thiadiazole Derivatives via Reagent-Based Cyclization of Thiosemicarbazide Intermediate. *J Org Chem* **2013**, *78* (2), 438-444. DOI: 10.1021/jo302324r.
- (32) Korosi, J. 4-Mono(disubstituted 1-isonicotinoyl thiosemicarbazides. Hungary HU148949, 1962.
- (33) Cansiz, A.; Orek, C.; Koparir, M.; Koparir, P.; Cetin, A. 4-Allyl-5-pyridin-4-yl-2,4-dihydro-3H-1,2,4-triazole-3-thione: Synthesis, experimental and theoretical characterization. *Spectrochim Acta A* **2012**, *91*, 136-145. DOI: 10.1016/j.saa.2012.01.027.

- (34) Abdel-Rhman, M. H.; Hussien, M. A.; Mahmoud, H. M.; Hosny, N. M. Synthesis, characterization, molecular docking and cytotoxicity studies on N-benzyl-2-isonicotinoylhydrazine-1-carbothioamide and its metal complexes. *J Mol Struct* **2019**, *1196*, 417-428. DOI: 10.1016/j.molstruc.2019.06.092.
- (35) Riccieri, F. M. P., Giuseppe A.; Castellani Pastoris, M. Thiourea derivatives and their antitubercular activity. *Farmaco, Edizione Scientifica* **1967**, *22* (2), 114-120.
- (36) Ceylan, S.; Bektas, H.; Bayrak, H.; Demirbas, N.; Alpay-Karaoglu, S.; Ulker, S. Syntheses and Biological Activities of New Hybrid Molecules Containing Different Heterocyclic Moieties. *Arch Pharm* **2013**, *346* (10), 743-756. DOI: 10.1002/ardp.201300161.
- (37) Iqbal, R. Z. K. R. N. H. Synthesis of 2,4-dihydro-4-(2-phenylethyl)-5-(isomeric pyridyl)-3H-1,2,4-triazole-3-thiones and their derivatives. *Turkish Journal of Chemistry* **1996**, *20* (4), 295-301.